Q. J. R. Meteorol. Soc. (2001), **127**, pp. 601–633

Coriolis effects on orographic and mesoscale flows

By J. C. R. HUNT[1]*, H. OLAFSSON[2] and P. BOUGEAULT[3]

[1]*CERFACS and IMFT, Toulouse and Arizona State University*

[2]*Icelandic Meteorological Service, Iceland*

[3]*CNRM, Météo-France, France*

(Received 21 December 1998; revised 1 August 2000)

SUMMARY

A perturbation theory is developed for the effects of rotation on stably stratified flow over mountains at low Froude number, $\mathbb{F} = U_0/(NH)$ where N is the buoyancy frequency, U_0 is the wind speed and H is the mountain height. The Rossby number, $\mathbb{R}_0 = U_0/(fD)$ where f is the Coriolis parameter, and D the along-wind length of the mountain, is assumed to be a large number. The mountain width, $\overline{\beta}D$, is assumed to be larger than D. Typically $\mathbb{R}_0$ is found to lie in the range 3–10. The results are compared with the recent numerical simulations. It is found that as the flow impacts on the mountain, in the northern hemisphere it turns to the left (with your back to the wind); also wave activity over the top of the mountain is greatest on the left side but the pressure drop is greatest on the right in the northern hemisphere. Over the Rossby deformation distance, L_R, of the order of HN/f, e.g. 150 km for the Pyrenees, a new wake structure develops that can extend downwind over 1000 km (or a spin-down distance). There is a momentum defect within the wake but the wind speed increases either side of the wake. Coriolis forces induce a deflection upwards of the isopycnals (and hence more precipitation) on the left, and downwards on the right; this is consistent with some of the differences in mesoscale weather and climate phenomena that are observed on the different flanks of elongated mountains and between the different side of wide valleys, and also in the wakes downwind of mesoscale convection cells. The large perturbation pressure change predicted by the theory is of the order of $\rho U_0^2/\mathbb{F}$ (where ρ is the density), which is consistent with the magnitude of the terms introduced into the recent European Centre for Medium-Range Weather Forecasts orographic parametrizations, but it should be noted that these large Rossby–Froude orographic effects on drag and wave flux are asymmetric with respect to the mountain's centre line. The theory shows how 'lift' forces on the mountain are caused, and how these are related to circulation in horizontal planes around the mountains.

KEYWORDS: Atmospheric dynamics Mountains Rotation

1. INTRODUCTION

Research into low-level atmospheric flows is not only necessary to improve numerical weather prediction and general circulation models but also for improving our insight into these flows to help forecasters and climatologists. The effects of mountains on weather over 500 km downwind is still not well understood. Qualitative accounts of mountain meteorology tend to focus on the balance between inertial effects, buoyancy forces caused by thermal stratification, turbulent shear stresses and boundary-layer effects such as separation (e.g. Scorer 1978). However, Manley (1952) comments that these effects do not satisfactorily explain some notable variations of British climate on scales of the order of 50 km, in particular their asymmetrical patterns over orography in relation to prevailing wind direction. Neither climatological textbooks nor forecasters' handbooks (Meteorological Office 1993) suggest that Coriolis forces affect the local meteorology on this scale.

The principal difficulty in the approximation of the effects of mountains in numerical weather prediction (NWP) or global circulation models (GCMs) is that many of the details of the mountains' shapes are too small to be represented by calculations on the coarse grids typical of global weather or climate models, currently ranging from 50 to 300 km. The theoretical models used as a basis of current subgrid-scale calculations were derived for flows where the Froude number ($\mathbb{F} = U_0/(NH)$) is greater than 1.0; here U_0 is the approach wind speed, N is the buoyancy frequency and H the height of the mountain. However, for most large mountains, where $H \sim 1$ km and $U_0 \lesssim 10$ m s^{-1},

* Corresponding author, present address: Departments of Space & Climate Physics and Geological Sciences, University College, Gower Street, London WC1H 0AH, UK.

$N \sim 10^{-2}\ \mathrm{s}^{-1}$, there are many situations where $\mathbb{F} \lesssim 1$ and where most of the flow below the mountain top has to pass round the mountain (Sheppard 1956).

To represent this parameter range Lott and Miller (1997) introduced into subgrid-scale orographic modelling some of the results of research into flow around mountains at low Froude number (e.g. Baines 1995). However, their derived algorithms for the total drag force on the flow, $\mathbf{F}_T^*$, do not formally account for the fact that in atmospheric flows over large mountain ranges rotational effects are also important, i.e. the Rossby number, $\mathbb{R}_0 \sim 1$–10 (Miller, private communication), where $\mathbb{R}_0 = U_0/(fD)$, f is the Coriolis parameter and D the along-wind length of the mountain.

Numerically this low-Froude-number parameter range has been studied by Peng Li *et al.* (1995) and Olafsson and Bougeault (1997; hereafter OB2) who considered cases where $\mathbb{R}_0$ is finite, and by Olafsson and Bougeault (1996; hereafter OB1) and Miranda and James (1992) for cases where $\mathbb{R}_0 = \infty$. The only theory with which they compared their data was the linear theory for $\mathbb{F} \gg 1$. They disregarded the asymptotic theory for $\mathbb{F} \to 0$ of Drazin (1961), because it did not account for any of the observed wave motion above the hill or for the separated flow.

Recently an approximate quantitative model has been proposed by Hunt *et al.* (1997; hereafter HFLGM) for $\mathbb{F} \ll 1$ that accounts for these omissions. It includes firstly an analysis of the wave motion and 'potential' vertical vorticity (or PV) 'banners' (Aekido and Schar 1998) generated in the thin top layer, [T], as if by a 'cut-off' hill whose thickness H^* is about equal to $\mathbb{F}H$. This theoretical estimate of Drazin (1961) has now been supported by many laboratory, field and numerical experiments, e.g. Snyder *et al.* (1985) and Smolarkiewicz and Rottuno (1989). The positive and negative PV in [T] is dynamically connected to the horizontal vortex flow in the separated wake flow of the middle layer, [M]. The value of H^* is determined by matching the asymmetric pressure distribution in these two layers. Most of the drag force $\mathbf{F}_T^*$, is produced by the separation-induced low pressure in [M], when $\mathbb{F} \ll 1$. The 'cut-off' hill approximation was used successfully for calculating mountain waves in the recent Mesoscale Alpine Project (Doyle, personal communication).

These mountain flows in the realistic parameter range $\mathbb{F} \ll 1$ and $1 \ll \mathbb{R}_0 < \infty$ are modelled here by approximating the shedding of vorticity into the wake by that from a porous mountain with distributed drag, a hypothesis first introduced by Taylor (1944) and developed by Newley *et al.* (1991; hereafter NPH). Shutts' (1998) orographic flow calculations based on semi-geostrophic theory for $\mathbb{F} \ll 1$, $R_0 > 1$ for inviscid flow, without allowing for the shed vorticity, are broadly consistent with the results derived here on the upwind side of the mountain.

The physical concepts and numerical results of flow around and downwind of a mountain also help explain the flow around convective systems (Browning and Ludlam 1962; Hunt *et al.* 1996), based on fluid mechanical studies of shedding of vorticity from jets and plumes in cross flows (e.g. Coelho and Hunt 1989).

Finally, the model enables us to derive an estimate for the transverse or 'lift' force produced by a mountain on the flow perpendicular to the approach flow direction (cf. Mason 1977; Smith 1979; Lott 1999). A report is available from the authors describing the mathematical analysis and the results in more detail.

2. General analysis for the far field of an isolated mountain

(*a*) *Assumption and nomenclature*

The main assumptions in the perturbation analysis (expressed in Cartesian coordinates defined in Figs. 1 and 2) for the strongly stratified rotation flow far from an isolated

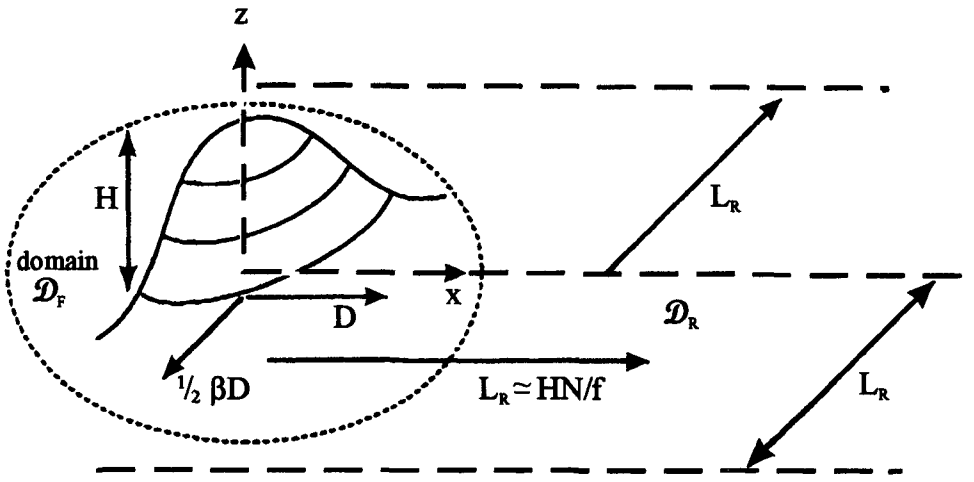

Figure 1. Definition sketches of the Froude and Rossby 'domains' $\mathcal{D}_F$, $\mathcal{D}_R$ for stably stratified flow over a mountain where the transverse width, $\frac{1}{2}\beta D$, is much less than the Rossby deformation distance, L_R. (The dimensionless Froude number is small and the Rossby number is large so that the boundary between $\mathcal{D}_F$ and $\mathcal{D}_R$ is far from the mountain.) See text for further details.

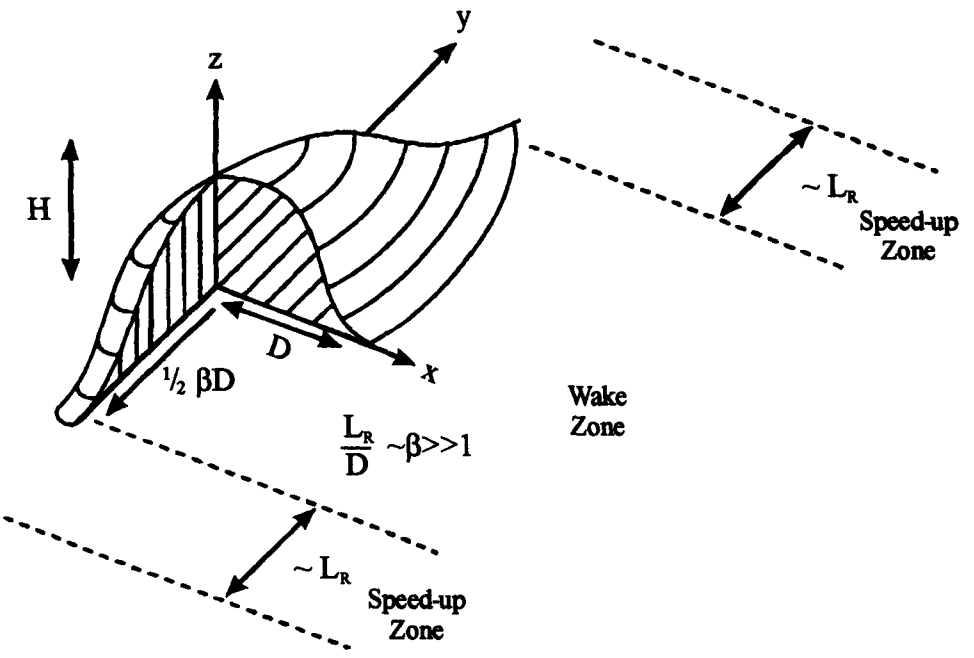

Figure 2. As Fig. 1, but here βD is much greater than L_R, so that Coriolis effects are significant near the mountain in $\mathcal{D}_F$.

mountain (or seamount) is that it is produced by effective along-wind and crosswind forces on the flow $\mathbf{F}_T^*$ and $\mathbf{G}_T^*$ and:

(i) the flow is incompressible and the Boussinesq approximation is valid (thus ignoring the compressibility effects considered by Smith (1979) and by OB2);

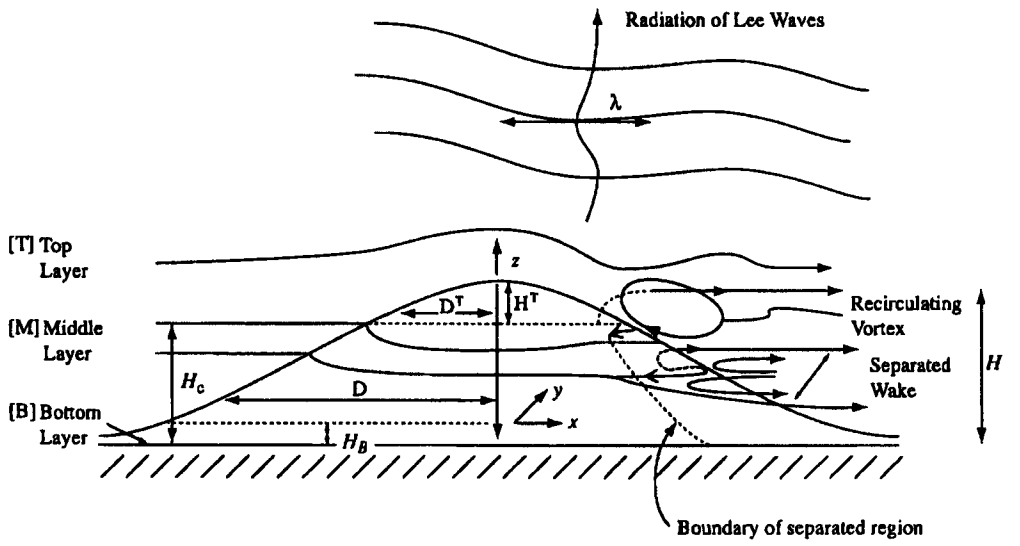

Figure 3. Definition sketch for flow over a mountain at low Froude number, i.e. $\mathbb{F} \ll 1$, in the Froude domain where rotational effects are negligible, i.e. $\mathbb{R}_0 \gg 1$ (from Hunt *et al.* (1997)). See text for details.

(ii) the upwind flow U_0 is uniform, so that shear effects on the mountain (which can be significant (cf. HFLGM) are neglected);

(iii) there is a uniform upwind density stratification $\rho_0(z^*)$ so that $N^2 = (-g\partial\rho_0/\partial z^*)/\rho_{00}$ is a constant, where $\rho_{00} = \rho_0(z^* = 0)$, Ω is the rotation rate and $f = 2\Omega$;

(iv) vorticity is generated near the mountain, and is advected downwind. This is effectively modelled as a distributed body force $\mathbf{R}^*$ per unit volume with along-wind and crosswind components (the effect of surface friction is discussed later in section 5);

(v) the parameter range is defined geometrically in terms of the maximum mountain height H, the half-length (in the flow direction) D, and breadth at each height $\beta(z^*)D$. Note $\overline{\beta} = \int_0^H \beta\, dz^*/H$. The inertial–buoyancy force balance is defined by $\mathbb{F}$ (based on the height H) or its inverse, the stratification parameter, $\mathbb{S}$,

$$\text{viz.} \quad \mathbb{F} = 1/\mathbb{S} = U_0/NH. \tag{1}$$

This parameter characterizes the flow in the Froude domain, $\mathcal{D}_F$, near the mountain, see Fig. 3. It is assumed that $\mathbb{F} \ll 1$, or $\mathbb{S} \gg 1$ in the analysis. Over large mountain ranges it is generally found that $0.1 < \mathbb{F} \lesssim 0.4$.

The inertial–rotational force balance is defined by the Rossby number or its inverse,

$$\text{viz.} \quad \mathbb{R}_0 = 1/\epsilon = U_0/fD \gg 1 (\sim 1\text{–}2.5). \tag{2}$$

It is assumed here that $\mathbb{R}_0 \gg 1$ or $\epsilon \ll 1$. Typically for the Pyrenees or Himalayas R_0 lies in the range 1–2.5.

H is assumed to be small compared to D. The Rossby deformation scale L_R $(= HN/f)$, which is assumed to be large compared to D, characterizes the flow far from the mountains in the Rossby domain, $\mathcal{D}_R$. Note that the dimensionless scale $\mathbb{L}_R = L_R/D \gg 1$. In the atmosphere if $H \sim$ 1–5 km, $L_R \sim$ 100–500 km $\sim 10D \sim 10^2 H$ for typical mountains. If the width $\overline{\beta}D$ is comparable with L_R then the flow in $\mathcal{D}_R$ affects the flow near the mountain in $\mathcal{D}_F$.

In our notation the total forces acting on the mountain are

$$F_T^*, G_T^* = \int_\infty^\infty \int_\infty^\infty \int_0^\infty \mathbf{R}^* \, dx^* \, dy^* \, dz^*, \tag{3a}$$

where the equivalent body force per unit volume is

$$\mathbf{R}^* = \frac{1}{D}\left(\frac{1}{2}\rho U_0^2\right)(F, G)(x, y, z), \tag{3b}$$

and $x, y, z = (x^*/D, y^*/D, z^*/H)$. Thence drag and 'lift' coefficients at each level (z) are related to the dimensionless width $\beta(z)$ (see Fig. 1) by

$$\begin{aligned}\int_{-\infty}^\infty \int_{-\infty}^\infty (|F|, |G|)\, dx\, dy &= \{C_D(z), C_L(z)\}\beta(z) \quad \text{for } 0 \leqslant z \leqslant 1 \\ &= 0 \quad \text{for } 1 < z.\end{aligned} \tag{3c}$$

These coefficients can be estimated from the calculated or measured pressure distribution around the mountain and its slope (Vosper and Mobbs 1997). In these calculations we only consider situations where the approach flow is normal to symmetrically shaped elongated mountains. This means that the main force on the flow is in the x direction, and G is much less than F. Because the calculations are linear the effects of G can be considered separately from those of F (as in sections 2(d), 3(c), 4, 5, and 6).

For calculating the flow upwind or downwind from the centre of the mountain outside the region of resistance where $|x| \gg 1$, only the integrated effect of the resistance needs to be considered, so that

$$F, G \simeq -\overline{C_D}, \overline{C_L}\delta(x)\{\hat{\hat{F}}(y, z), \hat{\hat{G}}(y, z)\} \quad \text{for } z \leqslant 1, \tag{3d}$$

where $\overline{C_D} = \int_0^1 C_D(z)\beta(z)\, dz$ and $\overline{C_L}$ are averaged values of C_D, $C_L(z)$ over the cross-section of the mountain (normal to the flow), and the delta function $\delta(x)$ and drag and lift variables $\hat{\hat{F}}$, $\hat{\hat{G}}$ are normalized so that

$$\int_{-\infty}^\infty \delta(x)\, dx = 1, \quad \int_0^1 \int_{-\infty}^\infty \begin{Bmatrix}\hat{\hat{F}} \\ \hat{\hat{G}}\end{Bmatrix} dy\, dz = 1. \tag{3e}$$

The orders of magnitude of $\overline{C_D}$, C_D and $\hat{\hat{F}}$, $\hat{F}$ and their variations with aspect ratio are estimated to be

$$\begin{aligned}&\overline{C_D} \sim C_D \sim 1 \text{ and } \hat{\hat{F}} \sim 1, \hat{F} \sim 1 \quad \text{if } \overline{\beta} \sim 1; \\ &\overline{C_D} \sim \beta \text{ and } \hat{\hat{F}} \sim 1/\overline{\beta} \quad \text{if } \overline{\beta} \gg 1.\end{aligned} \tag{3f}$$

For flow through a porous region where the velocity components are $U_0(1 + u, v, w)$ the normalized drag and lift distributions $\overline{C_D}\hat{\hat{F}}$ and $\overline{C_L}\hat{\hat{G}}$ are determined by the x and y components of the resistive force. This is proportional to the square of the local mean velocity at each location in the resistive region where the 'resistivity' (see NPH) is defined as χ_D in the x direction and χ_L in the transverse (y) direction

$$\overline{C_D}\hat{\hat{F}} = \chi_D(1 + u)\{(1 + u)^2 + v^2\}^{1/2}; \quad \overline{C_L}\hat{\hat{G}} = \chi_L v\{(1 + u)^2 + v^2\}^{1/2}. \tag{3g}$$

(*b*) *Governing equations*

Denoting dimensional perturbation variables as $(\,)^+$, the components of the velocity field are $U^* = (U_0 + u^+, v^+, w^+)$. The pressure perturbation is p^+ and density perturbation is ρ^+. Normalizing these variables on U_0, $\rho_{00}U_0^2$, $(\rho_{00}N^2H/g)$ respectively, normalizing the coordinates as in (3b), and invoking the 'hydrostatic' approximation because $D \gg H$ and $\mathbb{S} \gg 1$ (Gill 1982, p. 159), the linearized momentum equations for the time-averaged flow over the whole flow field, including the region of distributed resistance are

$$u_x = -p_x + \epsilon v + F \tag{4a}$$

$$v_x = -p_y - \epsilon u + G \tag{4b}$$

$$0 = -p_z - \mathbb{S}^2\sigma \tag{4c}$$

$$u_x + v_y + w_z = 0 \tag{4d}$$

$$\sigma_x = w, \quad \text{where } \sigma = -\rho^+/(\rho_{00}N^2H/g). \tag{4e}$$

Here F and G are defined in terms of u, v by (3g); σ is both density perturbation and the vertical streamline displacement. Note that from (4a), (4b) the perturbation to the vertical vorticity $\omega = v_x - u_y$, is given by:

$$\omega_x = \epsilon\sigma_{xz} - F_y + G_x. \tag{4f}$$

Then integrating, from far upstream (in both domains $\mathcal{D}_F$ and $\mathcal{D}_R$), we see that the normalized perturbation to the PV, $(\delta(PV)$ defined as $(\omega^* + f)(\partial\rho_{00}/\partial z + \partial\rho^+/\partial z))$ is

$$\delta(PV) = \omega - \epsilon\sigma_z = -\int_{-\infty}^{x} F_y \, dx + G. \tag{4g}$$

These coupled equations can be reduced to higher-order equations for each of the horizontal velocity perturbations (u, v) and the streamline displacement σ, in terms of F and G, as follows:

$$\mathcal{L}(u) = \int_{-\infty}^{x} F_{yy} \, dx + \frac{1}{\mathbb{S}^2}F_{zzx} + \left(\frac{\epsilon}{\mathbb{S}^2}G_{zz} - G_y\right) \tag{5a}$$

$$\mathcal{L}(v) = -F_y - \frac{\epsilon}{\mathbb{S}^2}F_{zz} + \frac{1}{\mathbb{S}^2}G_{xzz} + G_x \tag{5b}$$

$$\mathcal{L}(\sigma) = \frac{\epsilon}{\mathbb{S}^2}\int_{-\infty}^{x} F_{yz} \, dx - \frac{1}{\mathbb{S}^2}F_{zx} - \left(\frac{\epsilon}{\mathbb{S}^2}G_z + \frac{1}{\mathbb{S}^2}G_{yz}\right), \tag{5c}$$

and

$$u_x + v_y + \sigma_{zx} = 0, \tag{5d}$$

where the operator

$$\mathcal{L} = \nabla_{xy}^2 + \frac{\epsilon^2}{\mathbb{S}^2}\frac{\partial^2}{\partial z^2} + \frac{1}{\mathbb{S}^2}\frac{\partial^4}{\partial z^2 \partial x^2} \quad \text{and} \quad \nabla_{xy}^2 = \frac{\partial^2}{\partial x^2} + \frac{\partial^2}{\partial y^2}. \tag{5e}$$

The boundary conditions for these equations are that: (i) $\sigma = 0$ on $z = 0$; (ii) $\partial u/\partial x$, $\partial v/\partial x$, $v \to 0$ as $x^2 + y^2 \to \infty$; (iii) wave flux is upwards as $z \to \infty$ in $\mathcal{D}_F$, and $|\mathbf{u}| \to 0$ as $z \to \infty$ in $\mathcal{D}_R$; (iv) $|u| \to 0$ as $x \to -\infty$; but, because of the form of (5a),

$$|\mathbf{u}| \neq 0 \quad \text{as } x \to \infty. \tag{6}$$

Note that for a mountain that is symmetrical about its centre line ($y = 0$), F is symmetric to leading order. Therefore u is symmetric, while v and σ have antisymmetrical components. Since, from (3g), G depends on v, to first order it is non-zero and has symmetric and non-symmetric components.

(c) *Drag-induced perturbations for* $\mathcal{D}_F$

Consider the form of (5) away from the mountain but within a distance L_R, i.e. when $|x^2 + y^2| \gg 1$ but $(x^2 + y^2)/\mathbb{L}_R^2 \ll 1$. Then (below [T]) (5) becomes (to leading order) for the drag perturbations

$$\nabla_{xy}^2 \begin{Bmatrix} u \\ v \\ \sigma \end{Bmatrix} = \begin{Bmatrix} -\overline{C_D}\mathcal{H}(x)\hat{\hat{F}}_{yy}(y, z) \\ +\overline{C_D}\delta(x)\hat{\hat{F}}_y \\ +\dfrac{\overline{C_D}}{\mathbb{S}^2}\delta'(x)\hat{\hat{F}}_z \end{Bmatrix}, \tag{7a–c}$$

where $\mathcal{H}(x) = \int_{-\infty}^{x} \delta(x)\, dx$ is the Heaviside step function.

To understand the forms of the solutions for narrow and broad mountains (i.e. $\beta \ll 1$; $\beta \gtrsim 1$) we consider the simplest possible mountain with a rectangular cross-section whose resistance and approximate shape is given by $y = \pm\beta(z)/2$, $|z| < 1$. Then

$$\hat{\hat{F}} = (1/\overline{\beta})\{\mathcal{H}(y + \beta/2) - \mathcal{H}(y - \beta/2)\} \quad \text{where, to satisfy (3e)}, \overline{\beta} = \int_0^1 \beta\, dz. \tag{8}$$

We introduce a symmetric (image) solution below $z = 0$ in order to satisfy the boundary condition (6a) that $\sigma = 0$ on zero.

Using the standard Green's function solution for the two-dimensional Laplace's equation, (7a) leads to

$$u = -\frac{\overline{C_D}}{2\pi\beta}\left[\tan^{-1}\left(\frac{x}{y + \beta/2}\right) - \tan^{-1}\left(\frac{x}{y - \beta/2}\right) + \pi\left\{\mathcal{H}\left(y + \frac{\beta}{2}\right) - \mathcal{H}\left(y - \frac{\beta}{2}\right)\right\}\right]. \tag{9}$$

Thus in the central wake, where $|y| \ll \beta/2$, near the mountain, where $\beta \gg x > 0$, $u = -\overline{C_D}/2\overline{\beta}$; and further downwind where $x \gg \beta$, $u = -\overline{C_D}/\overline{\beta}$. See Fig. 4(a).

Since $\overline{C_D} \propto \overline{\beta}$, this shows how in the central wake u is independent of the aspect ratio β in this approximation. The solutions in (9) have previously been compared with bluff-body wakes for neutral and stratified flows (NPH).

Similar solutions show that to leading order, as with other bluff bodies, the maximum transverse velocities produced by the drag forces are antisymmetrical and occur at the outer edges of the mountain where $y = \pm\beta$.

Calculations for the vertical deflection of the streamlines show that they are negative far downwind (for most mountain shapes). This is consistent with usual low-Froude-number flow through a resistive region (e.g. NPH).

The pressure distribution in $\mathcal{D}_F$ for the [M] layer, which has a drop across the mountain associated with the drag, is given from (4a), $p = -u + \int_{-\infty}^{x} F\, dx$. So that for a mountain, whose resistance is as defined in (8), on $y = 0$,

$$p = \frac{\overline{C_D}}{\overline{\beta}}\left[\frac{1}{\pi}\tan^{-1}\{x/(\beta/2)\} + \left\{\frac{1}{2} - \mathcal{H}(x)\right\}\right]. \tag{10}$$

Thus $p \to 0$ as $|x|/\beta \to \pm\infty$.

(*d*) *Lift-induced perturbations in* $\mathcal{D}_F$

The lift force $G(\mathbf{x})$, which is proportional to the transverse velocity v, leads to a horizontal velocity perturbation, with components $u^{(L)}$, $v^{(L)}$, and a corresponding vertical vorticity $w^{(L)}$. The asymptotic expansions of u, v and $u^{(L)}$, $v^{(L)}$ have to be defined in powers of $\mathbb{S}^{-1}$ and ϵ, in order to match with the flow in $\mathcal{D}_R$, i.e. $v = v_0 + \mathbb{S}^{-1}v_1 + \cdots$.

The expression for the distributed lift force in (3g) shows that it depends on the transverse velocity component impinging on and passing through the porous mountain which is derived in section 3. It is convenient to expand G as a series:

$$G = -\overline{C_L}\delta(x)\hat{\hat{\hat{G}}}(x, y, z) = -\delta(x)[\overline{C_{L_0}}\hat{\hat{\hat{G}}}_0 + \mathbb{S}^{-1}\overline{C_{L_1}}\hat{\hat{\hat{G}}}_1 + \cdots]. \tag{11}$$

An approximate model for the variation of v is used (especially that describes its increase towards the edges) to calculate C_{L_0}, C_{L_1} and $\hat{\hat{\hat{G}}}$, namely

$$\overline{C_{L_0}} = v_0\chi_L \simeq v_{0_{mx}}\overline{C_D}\hat{\hat{\hat{F}}} \simeq v_{0_{mx}}\overline{C_D}/\beta \quad \text{and} \quad \hat{\hat{\hat{G}}}_0 = \tfrac{1}{2}\{\delta(y - \beta/2) - \delta(y + \beta/2)\} \tag{12a}$$

where $v_{0_{mx}} \simeq (\overline{C_D}/4\pi\beta)\ln(\beta^2)$ is the maximum value of v_0 in $\mathcal{D}_F$.

To the next order in $\mathbb{S}^{-1}$ we consider the lift caused by a net positive transverse velocity $\overline{v_1}$ over the mountain (and, for a porous mountain, through it) caused by the Coriolis effect in the far field. This is approximately equal to

$$\overline{v_1} \simeq \frac{\overline{C_D}}{2\pi\beta}\frac{\beta}{\sqrt{\{(\beta/2)^2 + \mathbb{L}_R^2\}}},$$

and varies little over the cross-section of the mountain. For wide mountains where $\beta > \mathbb{L}_R \gg 1$, $\overline{v_1} \simeq u_0/3$; therefore,

$$\overline{C_{L_1}} \simeq \overline{v_1}\overline{C_D} \quad \text{and} \quad \hat{\hat{\hat{G}}}_1 = \frac{1}{\beta}\{\mathcal{H}(y + \beta/2) - \mathcal{H}(y - \beta/2)\}. \tag{12b}$$

In the near field $\mathcal{D}_F$, the solution to (7a) for the leading-order term in $u^{(L)}$ is

$$u_0^{(L)} = +\frac{\overline{C_{L_0}}}{4\pi}\left\{\frac{(y - \beta/2)}{x^2 + (y - \beta/2)^2} - \frac{(y + \beta/2)}{x + (y + \beta/2)^2}\right\}. \tag{13}$$

This is consistent with (4g) which shows that negative and positive values of the transverse force G at $y = \pm\beta/2$ produce a negative and positive transverse vorticity at the edges of the mountain, i.e. a further slowing down over the mountain and speeding up outside the outer edges.

Since $\hat{\hat{\hat{G}}}_1$ is similar in form to $\hat{\hat{\hat{F}}}$, $u_1^{(L)}$ is the same as the solution to (7b) for v_0.

Then, far downwind the net lift force on the mountain produces a net change in vorticity around the mountain over a distance βD and a greater speed-up over the left side of the mountain and on the left side of the wake. The lift force also induces an extra cross-flow perturbation $v^{(L)}$. Over the mountain the leading-order antisymmetric term ($v_0^{(L)}$) causes amplification of the lateral and downwind velocity around the edges by about 1/6.

3. Solution for the Rossby domain

(a) *Re-scaling*

When the Coriolis terms in the equations are considered and $(x^2 + y^2)^{1/2} \sim \mathbb{L}_R \gg 1$, the horizontal coordinates require re-normalizing on the new scale (as in NPH), i.e. $X = (\epsilon/S)x$, $Y = (\epsilon/\mathbb{S})y$, since the vorticity shed into the wake by the mountain in the region $\mathcal{D}_F$ is advected downwind into $\mathcal{D}_R$. The analysis also covers the case where the width is so great, i.e. $\beta D \gg L_R$, that the mountain extends 'sideways' into $\mathcal{D}_R$. The expression (3d) has to be re-expressed in terms of the new coordinates (and a re-scaled delta function) as

$$F = -\overline{C_D}\left(\frac{\epsilon}{\mathbb{S}}\right)\delta(X).\hat{\hat{F}}_{(R)}(Y, z). \tag{14a}$$

For the case of mountains with uniform resistance across each level defined by (8)

$$\hat{\hat{F}}_{(R)} = \frac{1}{\overline{\beta}}\{\mathcal{H}(Y + \beta_R) - \mathcal{H}(Y - \beta_R)\}, \tag{14b}$$

where the re-scaled half width, β_R, is given by $\beta_R = \beta/2\mathbb{L}_R$, and $\overline{\beta} = \int_0^1 \beta\, dz$. Note that $\hat{\hat{F}} = 0$ for $z > 1$. For far-field calculations of u, v, it is convenient to assume a 'top-hat' mountain cross-section so that β is constant for $|z| < 1$, in which case $\overline{\beta} = \beta$.

(b) *Perturbations caused by the drag*

When the Froude number is very small (i.e. $\mathbb{S} \gg 1$), the far-field perturbation caused by the resistive drag (i.e. the component F of $\mathbf{R}^*$) is described by solutions which can be expanded as asymptotic series in powers of $\mathbb{S}^{-1}$. The leading terms for u, v, σ, p are respectively u_0, v_0, $\mathbb{S}^{-1}\sigma_0$, $\mathbb{S}p_0$.

Note that here we take the width of the mountains to be comparable with L_R, i.e. $\beta_R = O(1)$, whereas in NPH it was assumed that the width of the mountain is comparable to its length, so that $\beta_R = O(l/\mathbb{L}_R)$. From (5) and (14), these terms satisfy the following equations

$$\nabla_R^2[u_0, v_0, \sigma_0,] = \overline{C_D}\{\hat{\hat{F}}_{(R)YY}\mathcal{H}(X), -\hat{\hat{F}}_{(R)Y}\delta(X), \hat{\hat{F}}_{(R)Yz}\mathcal{H}(X), \}. \tag{15}$$

Also the continuity equation leads to

$$\partial u_0/\partial X + \partial v_0/\partial Y = 0 \quad \text{and} \quad \partial u_1/\partial X + \partial v_1/\partial Y = -\frac{\partial^2 \sigma_0}{\partial X \partial z}. \tag{16}$$

Note u_0, v_1, σ_1, p_1 are symmetric, while v_0, σ_0, p_0 are antisymmetric. From (4) it follows that in $\mathcal{D}_R$ (which excludes $\mathcal{D}_F$)

$$p_{0X} = v_0, \quad p_{0Y} = -u_0, \quad u_{0z} = \sigma_{0Y}, \tag{17a}$$

and for the first-order terms

$$u_{1Y} = -\sigma_{0Xz}, \quad p_{1X} = v_1 - u_{0X}, \quad \sigma_1 = -p_{1z}. \tag{17b}$$

Note that when calculating p in $\mathcal{D}_R$ and integrating (17) from far upwind we need to match with p in $\mathcal{D}_F$, as defined in (10). Equations (17) show that u_0, v_0 are in geostrophic balance with the asymmetric pressure p_0, but their accelerations cause inertial forces and thence an ageostrophic symmetric pressure field p_1. Note that to

leading order the perturbation velocity lies in horizontal planes (from (17a)), but to the next order the vertical velocity is significant.

We obtain analytical solutions for the case of a mountain with a top-hat drag profile defined by (14a) and (14b). The effects of lift forces are considered later. We find from the three-dimensional Green's function solution (following the method of NPH)

$$u_0 = +\frac{\overline{C_D}}{4\pi\beta}\sum_1^4 (-1)^{(j)}\mathcal{U}(X, Y^{(j)}, z^{(j)}), \tag{18a}$$

where, for the arguments $a = X$, $b = Y^{(j)}$, $c = z^{(j)}$, the function

$$\mathcal{U}(a, b, c) = \tan^{-1}(c/b) + \tan^{-1}\left\{\frac{ac}{b(a^2+b^2+c^2)^{1/2}}\right\}, \tag{18b}$$

and

$$\begin{aligned} Y^{(1)} = Y^{(2)} = Y + \beta_R, \quad Y^{(3)} = Y^{(4)} = Y - \beta_R, \\ z^{(1)} = z^{(4)} = z + 1, \quad z^{(2)} = z^{(3)} = z - 1. \end{aligned} \tag{18c}$$

In considering the first three terms of the series for the streamwise and transverse velocity components, one notes that u_1 is zero (if $G = 0$), but at second order $u_2 \neq 0$. The transverse components v_0, v_1, can also be expressed as a sequence of expressions:

$$v_k = -\frac{\overline{C_D}}{4\pi\beta}\sum_1^4 (-1)^{(j+1)}\mathcal{V}_k(X, Y^{(j)}, z^{(j)}) \quad k = 0, 1, \tag{19a}$$

where

$$\begin{aligned} \mathcal{V}_0(a, b, c) &= \ln(c + \sqrt{a^2+b^2+c^2}), \\ \mathcal{V}_1(a, b, c) &= \frac{-cb}{(c^2+a^2)(a^2+b^2+c^2)^{1/2}}, \end{aligned} \tag{19b}$$

and $Y^{(j)}$, $z^{(j)}$ are defined as in (18c).

The leading-order term for the pressure perturbation, defined by (17a), is calculated from u_0 using (18a), whence,

$$p_0(X, Y, z) = -\frac{\overline{C_D}}{4\pi\beta}\sum_1^4 (-1)^j \int_0^Y \mathcal{U}(X, Y^{(j)}, z^{(j)})\, dY. \tag{20}$$

Although this integral cannot be expressed in closed form, approximations to it can be derived. As $X \to -\infty$, $p_0 \to 0$, but as $X \to \infty$

$$p_0(y, z) \sim -\frac{\overline{C_D}}{4\pi\beta}\sum_1^4 (-1)^j \mathcal{P}_\infty(Y^{(j)}, z^{(j)}); \tag{21a}$$

where

$$\begin{aligned} d &= Y^{(j)}(Y = 0), \\ \mathcal{P}_\infty(b, c, d) &= b\tan^{-1}(c/b) - d\tan^{-1}(c/d) + \frac{c}{2}\ln\left(\frac{c^2+b^2}{c^2+d^2}\right). \end{aligned} \tag{21b}$$

The leading terms for the vertical displacement σ_0, σ_1, which are defined in terms of u_0 by (17a), follow from the expression (18a):

$$\sigma_i = +\frac{\overline{C_D}}{4\pi\beta}\left\{\sum_1^4 (-1)^{(j)} \sum_i (X, Y^{(j)}, z^{(j)})\right\} \quad \text{for } i = 0, 1, \tag{22a}$$

where

$$\sum_0 (a, b, c) = \frac{1}{2}\ln(b^2 + c^2) + \frac{1}{2}\ln\left(\frac{q-a}{q+a}\right), \tag{22b}$$

where $q = \sqrt{a^2 + b^2 + c^2}$ and

$$\sum_1 = \frac{ab}{(a^2 + c^2)(a^2 + b^2 + c^2)}. \tag{22c}$$

(c) *Descriptions of the solutions of the perturbations*

(i) *Streamwise perturbations.* The results (20) to (22) are applied to mountains with very elongated shapes where $\beta \sim \mathbb{L}_R \lesssim 1$. The results are presented in Figs. 4 and 5.

So that the results can be compared with those near the mountain in $\mathcal{D}_F$, the formulae are presented in the same normalized coordinates (x, y, z) used in section 2, which are scaled on D. On the symmetry plane $y = 0$

$$u_0 = -\frac{\overline{C_D}}{2\pi\beta}\left(\tan^{-1}\left\{\frac{\mathbb{L}_R(z+1)}{(\beta/2)}\right\} + \tan^{-1}\left\{\frac{\mathbb{L}_R(1-z)}{\beta/2}\right\}\right.$$
$$+ \tan^{-1}\left[\frac{x\mathbb{L}_R}{(\beta/2)\{(x^2 + (\beta/2)^2 + \mathbb{L}_R^2(z+1)^2\}^{1/2}}\right]$$
$$\left. + \tan^{-1}\left[\frac{x\mathbb{L}_R}{(\beta/2)\{(x^2 + (\beta/2)^2 + \mathbb{L}_R^2(z-1)^2\}^{1/2}}\right]\right). \tag{23}$$

In the case where the width of the mountain is comparable with the Rossby radius, i.e. $\beta \gtrsim \mathbb{L}_R$, from (23) it follows that when

$$\mathbb{L}_R < \beta \ll x, \quad u_0 = -\frac{\overline{C_D}}{2\beta}. \tag{24}$$

However we note that the *magnitude* of the defect on the centre line (for given $\overline{C_D}/\beta$ which is independent of β) is about 50% of the value of that for a rounded mountain where $u_0 = -(\overline{C_D}/\beta)$.

It is at the edges of the wake where the main differences occur with wakes in non-rotating flows and in rotating flows, where the mountains are rounded. Just inside the wake edge on the surface, at $z = 0$, where

$$\beta/2 \gg (\beta/2 - y) > 0,$$
$$u = -\frac{\overline{C_D}}{2\pi\beta}\left\{\pi + \tan^{-1}\left(\frac{\mathbb{L}_R}{\beta}\right) + \tan^{-1}\left(\frac{x\mathbb{L}_R}{\beta\sqrt{x^2 + \beta^2 + \mathbb{L}_R^2}}\right)\right\}. \tag{25a}$$

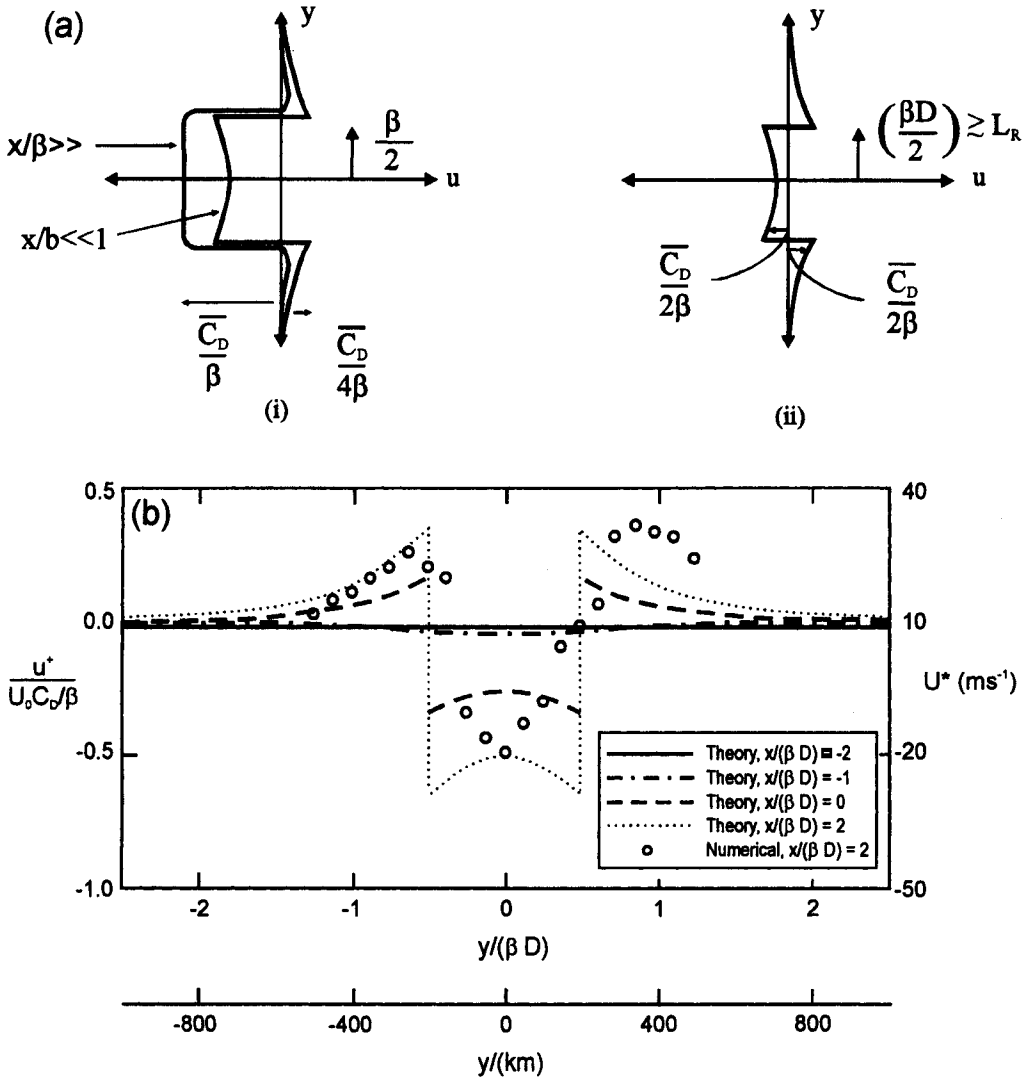

Figure 4. Theoretical profiles of the along-wind velocity perturbation, u^+, in the wake at $z = H/2$: (a) showing schematically the transition from their generally negative form (i) in the Froude domain, $\mathcal{D}_F$, to their form (ii) in the Rossby domain, $\mathcal{D}_R$, (when $\beta \gg \mathbb{L}_R$) where the peak negative value occurs near the edge and there is a positive speed-up outside the wake; (b) comparisons between results from the perturbation theory for a rectangular mountain and computations of Olafsson and Bougeault (1997) for a smooth ellipsoidal shaped mountain assuming $L_R/(\beta D) = 0.5$ and $C_D/\beta = 6$. The right-hand axis gives the full wind speed, U^*, assuming $U_0 = 10$ m s^{-1}; (c) maximum positive velocity perturbation outside the wake in $\mathcal{D}_R$. See text for details.

So that near the mountain, where $x \simeq 0$, if $\beta/2 = \mathbb{L}_R$,

$$u_0 = -\frac{\overline{C_D}}{\beta}\left\{\frac{1}{2} + \frac{1}{2\pi}\tan^{-1}(1/2)\right\} \simeq -0.57\overline{C_D}/\beta, \tag{25b}$$

and, very far downwind, where $\beta/2 \ll x$,

$$u_0 = -\frac{\overline{C_D}}{\beta}\left\{\frac{1}{2} + \frac{1}{\pi}\tan^{-1}(1/2)\right\} = -0.64\overline{C_D}/\beta, \tag{25c}$$

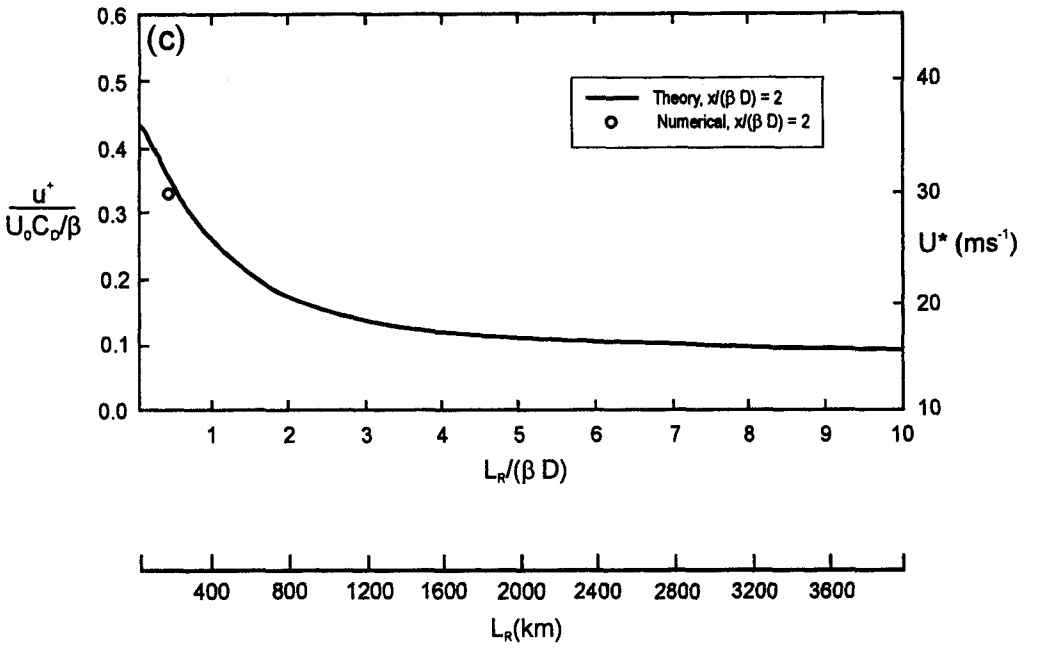

Figure 4. Continued.

see Fig. 4(a)(i) and (ii). Thus very close to the mountains (i.e. $x = 0$) and far downwind the difference between the edge and centre-line defects is less than 30%. But the solutions (24) and (25a) also show that over a downwind distance comparable to L_R the edge defect is 100% greater than the centre-line defect. At the outside edge of the wake where

$$\beta/2 \gg (y - \beta/2) > 0,$$

$$u_0 \simeq \frac{\overline{C_D}}{2\pi\beta}\left[\pi - \tan^{-1}\left(\frac{\mathbb{L}_R}{\beta}\right) - \tan^{-1}\left\{\frac{x\mathbb{L}_R}{\beta(x^2+\beta^2+\mathbb{L}_R^2)^{1/2}}\right\}\right]. \tag{26a}$$

This means that near the mountain where $x \ll \beta/2 \simeq \mathbb{L}_R$ and very far from the mountain, where $\beta/2 \simeq \mathbb{L}_R \ll x$,

$$u_0 = 0.43\frac{\overline{C_D}}{\beta}, \quad 0.36\frac{\overline{C_D}}{\beta}, \tag{26b}$$

respectively. Figure 4(c) shows the variation of the maximum speed-up with $\mathbb{L}_R$.

Thus for wide mountains the flow speeds up outside the wake; in the limit of a mountain much wider than the Rossby radius (i.e. $\beta \gg \mathbb{L}_R$) the velocity excess could be as large as the defect ($\simeq\overline{C_D}(1/2\beta)$). But for the case considered here, where $\beta/2 \simeq \mathbb{L}_R$, comparing (25c) and (26b) shows that the excess velocity very far downwind is about 50% of the maximum defect. Note that the *magnitude* of the maximum speed-up is independent of f, but its location is not.

Inspection of (20) shows that, as on the centre line, there is a significant decrease both in the defect and in the speed-up near the mountain top. Both continue to decrease upwards to a height of the order of $x/\mathbb{L}_R$ (see NPH). This forms the characteristic 'hyperbolic' wake of a mountain in a stably stratified rotating flow.

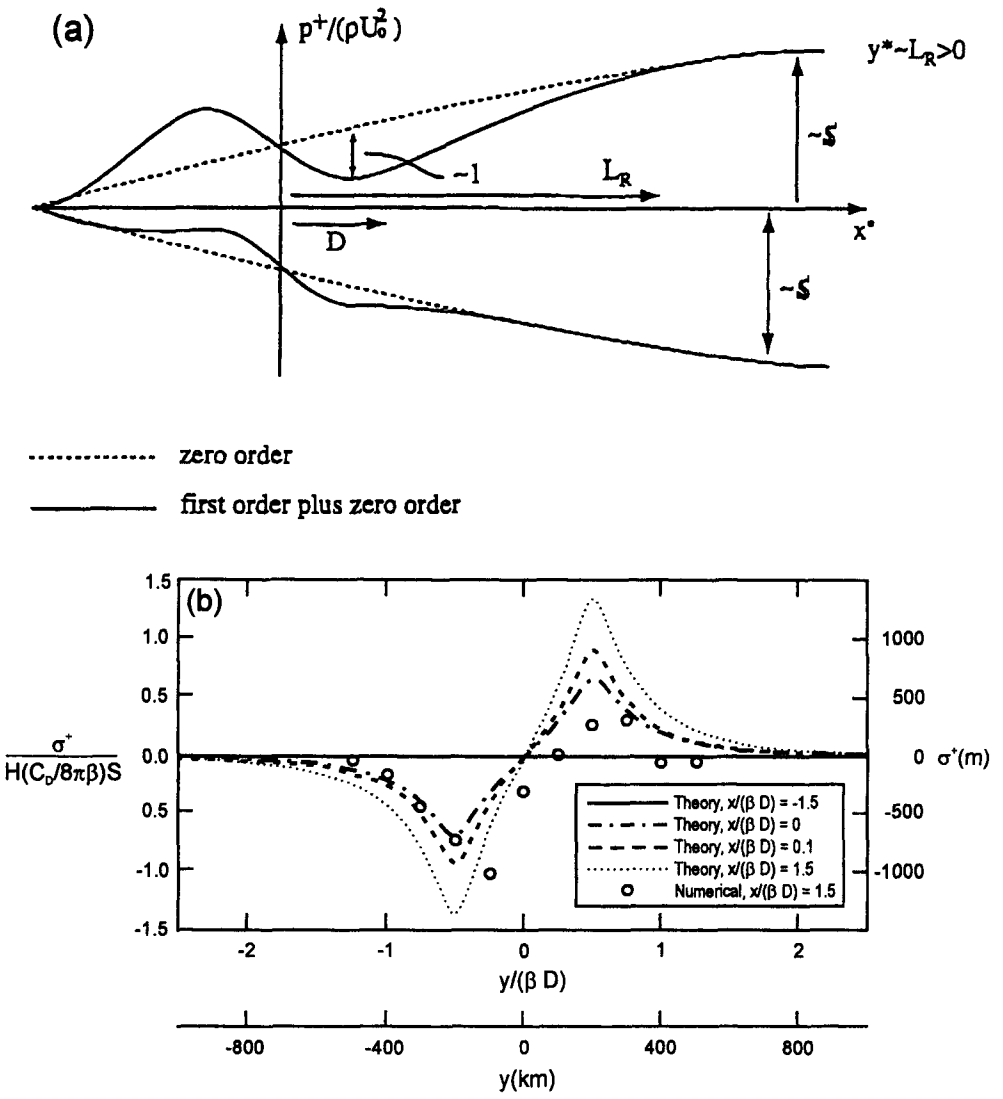

Figure 5. Theoretical pressure perturbations and vertical deflections in the wake, showing how the largest effects are asymmetric and persist downwind (with low pressure on the right). (a) pressure including the symmetric first-order terms which decay in a distance of the order of L_R; (b) vertical deflection in the Rossby domain (perturbation theory and computation of OB2). See text for details.

(ii) *Transverse velocity perturbation.* The solutions (19) for the first two terms of the expression for v can be simplified. For very wide mountains ($\beta/2 \gg \mathbb{L}_R$) on the plane $z = 0$ (for $x^2 + y^2 \gg \mathbb{L}_R^2$)

$$v_0 \simeq \frac{\overline{C_D}}{2\pi\beta} \cdot \mathbb{L}_R \cdot \left\{ \frac{-1}{\sqrt{x^2 + (y + \beta/2)^2}} + \frac{1}{\sqrt{x^2 + (y - \beta/2)^2}} \right\}. \tag{27}$$

Thus the maximum lateral velocity at the edges of the mountain, where $y \simeq \pm\beta/2$, is of the order of $C_D U_0$.

When $\sqrt{x^2 + y^2} \ll \mathbb{L}_R$, and when the hill's width is less than the Rossby scale (i.e. $\beta/2 \ll \mathbb{L}_R$), the expression (27) matches with the leading-order term in $\mathcal{D}_F$.

In both domains (for all values of the ratio $\beta/(2\mathbb{L}_R)$), at all downwind planes, the cross wind velocity (v_0) has its largest value at, or downwind of, the edge of the mountain where $y = \pm\beta/2$. Near the mountain's centre (where $|x| \ll 1$), v_0 has its maximum value for rounded mountains, i.e. where

$$\beta \lesssim \mathbb{L}_R, \quad v_{0_{mx}} \simeq \frac{\overline{C_D}}{2\pi\beta} \ln(\sqrt{1+\beta^2}). \tag{28}$$

But $v_{0_{mx}} \simeq (\overline{C_D}/2\pi\beta)\ln(\mathbb{L}_R)$ when $\beta \gg \mathbb{L}_R$; this is significantly larger than the maximum velocity defect $u_{0_{mx}}$ given by (25).

In terms of the downwind variations, v_0 is maximum on the plane $x = 0$, and in $\mathcal{D}_R$ decreases with distance in proportion to r^{-2} (where $r^2 \simeq x^2 + y^2$), as compared to the slower decay rate of r^{-1} in $\mathcal{D}_F$. This is because in $\mathcal{D}_R$, v_0 decreases with height over a distance $z \sim \sqrt{x^2+y^2}/\mathbb{L}_R^2$, i.e. within the 'wake' referred to above.

The first-order term for the cross-flow v_1 (or 'barrier jet'; Shutts 1998) is symmetric, and decays downstream to zero. Thus the largest value of the cross-flow is at the origin, where

$$v^+ = U_0 \mathbb{F} v_1(0, 0, 0) = \frac{U_0 \overline{C_D} \mathbb{F}}{2\pi\beta} \cdot \frac{\beta}{\sqrt{(\beta/2)^2 + \mathbb{L}_R^2}}. \tag{29}$$

v_1 increases until the width of the mountain is comparable with $\mathbb{L}_R$ (for given C_D/β).

Near the mountain, where $|x| \ll 1$, v_1 has its maximum value towards the top of the mountain but further upstream or downstream it is near the surface.

From (27) it follows that the horizontal deflections of the streamlines are of the order of L_R, and are at a maximum at the edge of the mountain. NPH showed how the lateral deflection of the streamlines Δy_ψ normalized on D can be calculated from the perturbation solution. From (19) it can be shown that far downwind to leading order, the asymmetric and symmetric components of Δy_ψ are given by:

$$\Delta y_\psi(x \to \infty, y, z = 0) = \int_{-\infty}^{\infty} v_0 \, dx + (\mathbb{S}^{-1})\Delta y_{\psi(1)}, \tag{30}$$

where

$$\Delta y_{\psi(0)} = \int_{-\infty}^{+\infty} v_0 \, dx \quad \text{and} \quad \Delta y_{\psi(1)} = \int_{-\infty}^{+\infty} v_1 \, dx;$$

both terms are of order $(\overline{C}_D/\beta)\mathbb{L}_R$, when $\beta \sim \mathbb{L}_R$, but only the latter produces a significant net displacement along the centre line.

(iii) *Pressure.* In the far field when $x/\mathbb{L}_R \to \infty = 0$,

$$p_0(\infty, y, z) \simeq \frac{\overline{C_D}}{4\pi\beta}\left[2\frac{(y+\beta/2)}{\mathbb{L}_R}\tan^{-1}\left(\frac{\mathbb{L}_R}{y+\beta/2}\right) - 2\frac{(y-\beta/2)}{\mathbb{L}_R}\tan^{-1}\left(\frac{\mathbb{L}_R}{y-\beta/2}\right) + \ln\left\{\frac{\mathbb{L}_R^2 + (y+\beta/2)^2}{\mathbb{L}_R^2 + (y-\beta/2)^2}\right\}\right]. \tag{31}$$

Note that on $x = 0$, p_0 is exactly one half of this value, i.e. $p_0(0, y, z) \simeq \frac{1}{2}p_0(\infty, y, z)$. Also note that for wide mountains where $\beta/2 \simeq \mathbb{L}_R$, p_0 has a maximum and

minimum value $p_{0_{\max,\min}}$ where $y \simeq \pm\beta/2$,

$$p_{0_{\max,\min}}(\infty, y = \pm\beta/2, 0) = \pm\frac{\overline{C_D}}{4\pi\beta}\left\{\frac{2\beta}{\mathbb{L}_R}\tan^{-1}\left(\frac{\mathbb{L}_R}{\beta}\right) + \ln\left(1 + \frac{\beta^2}{\mathbb{L}_R^2}\right)\right\}. \quad (32)$$

For more rounded shapes these maximum/minimum positions are closer to the centre. The pressure decreases outside the wake on a length-scale L_R irrespective of the width of the mountain. The vertical decrease of p_0 with height has a similar profile to that of u_0.

In order to estimate how p_0 varies in the wake, an approximation to the integral (22a) can be constructed. This is because u_0 does not vary rapidly, either across or along the wake, so that it can be averaged between the centre line and edge values. For a wide mountain where $\beta/2 \gtrsim \mathbb{L}_R$

$$p_0(x, y, z) \simeq -\left(\frac{y}{\mathbb{L}_R}\right)\frac{1}{2}\{u_0(x, y = 0, z) + u_0(x, y = \beta/2, z)\} \quad \text{for } x > 0,\ |y| \leqslant \beta/2 \quad (33a)$$

$$p_0(x, y, z) \simeq \frac{2}{\pi}\tan^{-1}\left(\frac{\mathbb{L}_R}{|y| - \beta/2}\right)\cdot p_0((x, |y| = \beta/2, z) \quad \text{for } x > 0,\ |y| > \beta/2. \quad (33b)$$

Upwind of the mountain the pressure decays with x also on a length-scale L_R so

$$p_0(x, y, z) \simeq \frac{2}{\pi}\tan^{-1}\left(\frac{\mathbb{L}_R}{x}\right)p_0(x = 0, y, z). \quad (33c)$$

Thus the leading-order pressure perturbation in $\mathcal{D}_R$ is positive everywhere for $y > 0$ and negative for $y < 0$. It rises continuously until it reaches its asymptotic value where $x \sim \mathbb{L}_R$.

In a dimensional form, the first-order pressure term p_1 in $\mathcal{D}_R$ is of the same order (namely $\rho U_0^2\overline{C_D}$) as the leading-order pressure in $\mathcal{D}_F$ and, therefore, they should match near the mountain. (We recall that the leading-order pressure changes are much larger than the pressure changes near the mountain.) As explained earlier, p_1 is calculated most simply by including the body force in the equation for $\mathcal{D}_R$. It follows that the integral of (17b) is

$$p_1(x, y, z) = \frac{1}{\mathbb{L}_R}\int_{-\infty}^{x} v_1\,dx - u_0 + \int_{-\infty}^{x} F\,dx. \quad (34)$$

Integrating this expression, we find:

$$p_1, (x, 0, 0) = \frac{\overline{C_D}}{\beta}\left(\frac{1}{\pi}\tan^{-1}\left\{\frac{x\beta/(2\mathbb{L}_R)}{\sqrt{\mathbb{L}_R^2 + (\beta/2)^2 + x^2}}\right\} + \frac{1}{\pi}\tan^{-1}\{\beta/(2\mathbb{L}_R)\}\right.$$
$$\left. + \frac{\tan^{-1}}{\pi}\left(\frac{\mathbb{L}_R}{\beta/2}\right) + \frac{1}{\pi}\tan^{-1}\left[\frac{x\{\mathbb{L}_R/(\beta/2)\}}{\sqrt{x^2 + (\beta/2)^2 + \mathbb{L}_R^2}}\right] - \mathcal{H}(x)\right). \quad (35a)$$

Note that this is consistent with the drag, i.e. $\iint\{p(x \simeq -1) - p(x \simeq +1)\}\,dy\,dz = \overline{C}_D$. Also $p_1(x, 0, 0) \to 0$ as $(x/\mathbb{L}_R) \to -\infty$.

Since $\tan^{-1} a + \tan^{-1}(1/a) = \pi/2$, as $|x|/\sqrt{\mathbb{L}_R^2 + (\beta/2)^2} \to \infty$, the net *pressure rise* along the centre line is zero, i.e.

$$p_1(\infty, 0, 0) \sim 0. \tag{35b}$$

Thus for very wide mountains, where $\beta \gg \mathbb{L}_R$ and $u_0(x, 0, 0) \to 0$, (35) shows that on the centre line the rise in pressure over the whole length of $\mathcal{D}_R$ caused by the turning of the wind (i.e. $\int_{-\infty}^{+\infty} v_1 \, dx$) is much greater than the effect of the streamwise deceleration (i.e. $-u_0$), and exactly balances the drag force ($\int_{-\infty}^{x} F \, dx$).

(iv) *Vertical deflection.* Where $x \gg \mathbb{L}_R$:

$$\sigma_0(\infty, y \cdot z) = -\frac{\overline{C_D}}{4\pi\beta} \cdot \frac{1}{2}\left[\ln\left\{\frac{(y+\beta/2)^2 + \mathbb{L}_R^2(z+1)^2}{(y+\beta/2)^2 + \mathbb{L}_R^2(z-1)^2} \cdot \frac{(y-\beta/2)^2 + \mathbb{L}_R^2(z-1)^2}{(y-\beta/2)^2 + \mathbb{L}_R(z+1)^2}\right\}\right]. \tag{36}$$

Note that, to leading order, the vertical displacement is antisymmetric. Also note (as with pressure) the airflow rises/falls as much upwind as downwind of the mountain i.e. $\sigma_0(x = 0, y, z) = \frac{1}{2}\sigma_\infty(\infty, y, z)$; see Fig. 5(a) and (b).

The maximum/minimum values (which are singular for our particular idealization of the hill's resistance, even far downwind of the mountain) occur where $y = \pm\beta/2$, $z \to 1$.

$$\sigma_{0_{\max,\min}} \sim \pm\frac{\overline{C_D}}{4\pi\beta}\left[\frac{1}{2}\ln\left\{\frac{(z-1)^2}{4}\right\} + \frac{1}{2}\ln(1 + 4\mathbb{L}_R^2/\beta^2)\right]. \tag{37a}$$

In reality the solution near the mountain where $z \sim 1$, is determined by the [T] layer with thickness $\mathbb{F}H$, so that

$$\sigma_{0_{\max,\min}} \sim \pm\frac{\overline{C_D}}{4\pi\beta}\{\ln(2/\mathbb{F})\}. \tag{37b}$$

Near the tops of very elongated mountains, where $\beta/2 \gg \mathbb{L}_R$, as $x/\mathbb{L}_R \to \infty$

$$\sigma_0 \sim \frac{\overline{C_D}}{2\pi}\mathbb{L}_R^2\left\{\frac{1}{(y+\beta/2)^2} - \frac{1}{(y-\beta/2)^2}\right\}, \tag{38}$$

except very close to the edge (within one half length), when (37b) is the local solution. Note that when $|y| \gg \beta/2$, in this case too, $\sigma_0 \propto (|y|)^{-3}$. The first-order displacement σ_1, given by (23) is symmetrical in y. The decrease of σ_1 downwind when $x \gg \mathbb{L}_R$ and $x \gg \beta/2$, is given by

$$\sigma_1 \sim -\left(\frac{\overline{C_D}}{\pi\beta}\right) \cdot 3xz\mathbb{L}_R^3(\beta/2)/(x^2 + \mathbb{L}_R^2 z^2)^{5/2}. \tag{39}$$

The height at which σ_1 reaches its maximum value z_{mx} is of the order of $x/\mathbb{L}_R$.

(*d*) *Velocity perturbation caused by 'lift forces'*

If the first two terms of the asymptotic expansion for G defined in section 2(d) are substituted into (14) for $\mathcal{D}_R$ and the same expansion of the lift affected components $u^{(L)}$

is applied, then

$$u_i^{(L)} = -\frac{1}{4\pi}\left\{\sum_1^4 (-1)^{j+1}\overline{C}_{L_i}\mathcal{U}_i^{(L)}(X, Y^{(j)}, z^{(j)})\right\} \quad i = 0, 1 \tag{40a}$$

where

$$\mathcal{U}_0^{(L)} = \frac{bc}{(a^2+b^2)(a+b^2+c^2)^{1/2}}, \quad \mathcal{U}_1^{(L)} = \ln(c+\sqrt{a^2+b^2+c^2}), \tag{40b}$$

and a, b, c are defined in terms of X, Y, z in (18b), and $\overline{C}_{L_0}$, $\overline{C}_{L_1}$ are defined in (11).

Thus, as in $\mathcal{D}_F$, the resistive forces at the edge of the mountain induce an extra symmetric velocity defect within the wake. But now, because of Coriolis effects, these forces produce a velocity speed-up outside the wake if the mountain is wide (i.e. $\beta \gtrsim \mathbb{L}_R$). But, unlike the speed-up produced by the drag forces, this lift-induced speed-up decays downwind when $x \gg \beta/2$.

The asymmetric first-order term $u_1^{(L)}$ is proportional to the leading-order transverse velocity v_0, so that using the solution (30b) and the estimate of C_{L_1} in (16b) leads to an acceleration of the flow in the streamwise direction upwind of the hill, reaching a maximum at $x = 0$. Thus $u^{(L)}$ contributes to the speed-up at the edge of the mountain (where $y \simeq \beta/2$) by about

$$\frac{1}{\mathbb{S}}\frac{\overline{C}_{L_1}}{2\pi\beta}\{\ln(\sqrt{1+\beta^2}), \ln \mathbb{L}_R\} \quad (\text{for } \beta \ll \text{or} \gg \mathbb{L}_R \text{ respectively})$$

and reduces the speed-up over the right-hand half of the mountain with a maximum value near the edge. In the case of very wide mountains, where $\beta > \mathbb{L}_R \sim 10$ and $C_{L_1} \sim \frac{1}{3}\cdot\overline{C_D} \sim \frac{1}{3}\cdot\beta U_0$, this asymmetric speed-up is of the order of U_0.

This asymmetric speed-up decreases downwind over a distance of the order of $\mathbb{L}_R$, when the streamwise perturbation velocities in the wake flow become more symmetric.

One of the implications of the significant asymmetry in the streamwise speed-up over the mountain with higher speed where $y > 0$, is that the local streamwise velocity $U_0(1+u+u^{(L)})$ and therefore the local Froude number $U^*/(NH)$ are both greater on the left-hand side of the mountain where $y > 0$. This leads to a deeper top layer [T] and stronger lee wave motion in the top layer on the left-hand side.

4. PHYSICAL INTERPRETATION OF THE MAIN RESULTS

The complicated pattern of perturbations to a stratified rotating flow caused by a porous mountain (and, by extension, a solid mountain) can be explained with the aid of the schematic diagrams in Figs. 6 and 7 showing the flow patterns and vectors of the vertical vorticity ω.

The terms in (4g) correspond to three quite clear contributions, which are expressed in terms of the changes to ω_z and to the change in the PV, $\Delta(PV)$,

$$\underset{\substack{\text{Perturbation}\\\text{vorticity}}}{\Delta\omega} = \underset{\substack{\text{Vorticity}\\\text{stretching}}}{\Delta\omega_S} + \underset{\substack{\text{Shed vorticity}\\\text{caused by}\\\text{resistive force}}}{\Delta\omega_D} + \underset{\substack{\text{Bound vorticity}\\\text{caused by a}\\\text{transverse force density}}}{\Delta\omega_L}. \tag{41a}$$

Note that the change in PV along streamlines is given by

$$\Delta(PV) = \Delta\omega - \Delta\omega_S. \tag{41b}$$

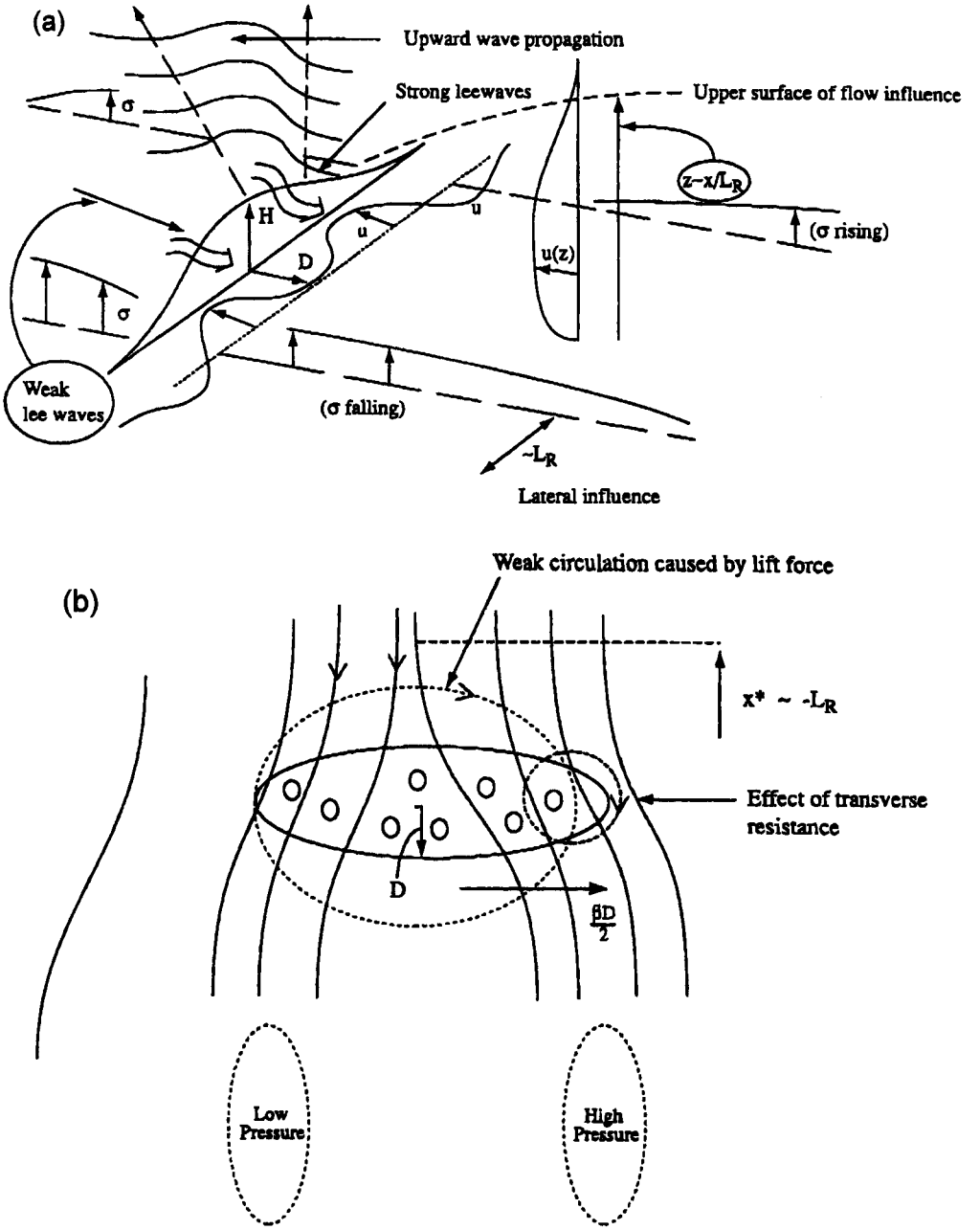

Figure 6. Schematic diagram of the significant Coriolis affected perturbations around mountain flows when the Froude number $\mathbb{F} \ll 1$ and the Rossby number $\mathbb{R}_0 \gg 1$: (a) three-dimensional sketch, (b) plan view. See text for definitions and discussion.

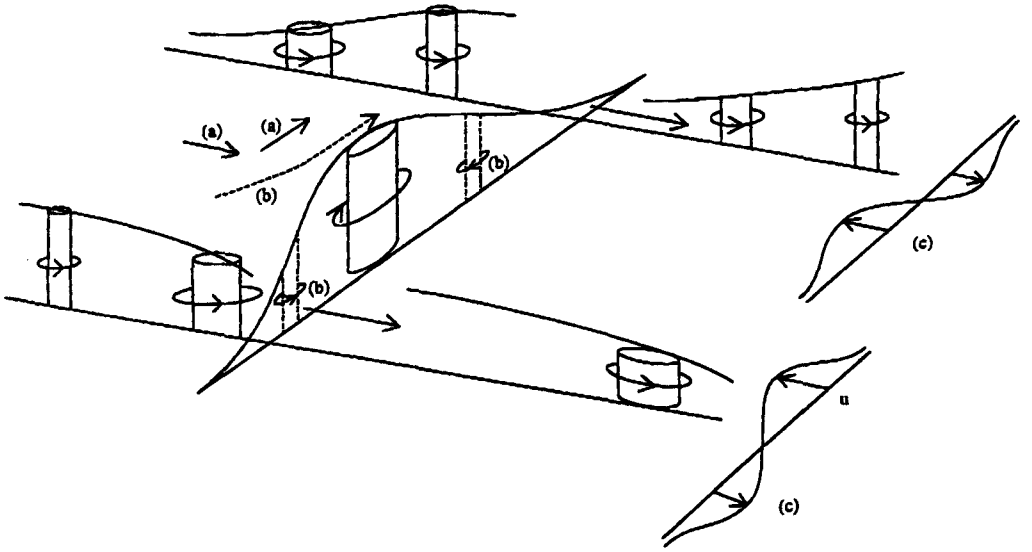

Figure 7. Schematic diagram of the perturbation of vertical vorticity around a mountain when the Froude number $\mathbb{F} \ll 1$, and the Rossby number $\mathbb{R}_0 \gg 1$, showing vorticity from earth's rotation $\Delta\omega_s$, shed vorticity $\Delta\omega_D$, caused by drag forces, and vorticity $\Delta\omega_L$, arising from lift or transverse forces. Note: streamwise and cross-stream accelerations designated (a) are caused by the stretching $\Delta\omega_s$ in $\mathcal{D}_R$ in the approach flow; those designated (b) are the streamline deflections in $\mathcal{D}_F$, caused by rotation and drag and by the bound vorticity $\Delta\omega_L$, including that caused by local edges; (c) shows changes in streamwise perturbation caused by $\Delta\omega_s$ and $\Delta\omega_D$. See text for definitions and discussion.

Here the first two mechanisms in (41) play a significant role outside the immediate region of the mountain or region of resistance, but the second mechanism is only significant downwind of the resistance because this is the only region, i.e. the wake, where there exists shed vorticity and therefore a change in PV. The third term is only non-zero within the body for a porous body, or on the surface of the body for certain solid bodies. This vorticity field induces a net circulation field around the mountain if there is a net sideways force acting on the mountain, i.e. a lift. This circulating velocity in the x–y plane decreases away from the mountain. We return to the explanation of $\Delta\omega_D$ and $\Delta\omega_L$ as part of our description of the flow.

Note that this equation is not sufficient in itself to explain everything! We also use where relevant the momentum equations (4).

As the flow approaches the mountain, its resistance (or blockage) causes u to decrease ($u < 0$) and the pressure to rise. Because of the slow decay ($u \propto r^{-1}$) of the perturbation, near the mountain even small Coriolis effects (i.e. $\mathbb{R}_0 \gg 1$) cause the perturbation pressure to be very large; this means that the perturbation field has to decrease faster over the Rossby deformation length L_R. Also, as a result of Coriolis forces there is a positive lateral pressure ($\partial p/\partial y > 0$). This produces an upward displacement of streamlines of $O(\mathbb{S}^{-1}H)$ on the left-hand side of the mountain and a downward displacement on the right. This causes an asymmetric vortex-stretching so that

$$\Delta\omega_s \simeq \pm\frac{(H/D)}{(NH/U)} \cdot \epsilon \quad \text{for } y \gtrless 0$$

upwind of the mountain, the other two vorticity generation terms in (41) being zero. This in turn distorts the flow, so that the blocking (i.e. $-u$) is decreased and the barrier jet (i.e. $|v|$) is increased as a result of the Coriolis effect upwind of the mountain. Even if the

width of the mountain is significantly greater than L_R (i.e. $\beta \gg \mathbb{L}_R$), the upwind flow is weakly blocked by the mountain over a distance upwind of the order of βD, but the most intense blocking and the formation of the barrier jet occurs along the upwind side of the mountain within a narrow region q, of width $\mathbb{L}_R$ ($\sim$100 km) in the flow direction (Shutts 1998).

The vorticity continuously shed from the mountain in the [M] layer is advected downwind and is confined to the wake. It is not suppressed by stable stratification, and therefore $\Delta\omega_D$ is the main contribution to ω in the wake. Its magnitude is effectively determined by the drag. However, the stretching of the vertical vorticity, $\Delta\omega_s$, depends on the dynamical interaction set up by $\Delta\omega_D$. As with the upwind flow, the transverse or geostrophic pressure gradient generated by Coriolis forces, i.e. ($\partial p/\partial y > 0$), is balanced hydrostatically by vertical displacements ($\partial\sigma/\partial y > 0$). The main linear effects are the stretching of the background vorticity to produce positive/negative $\Delta\omega_s$ either side of the wake (these could be described as 'banners' of enhanced PV resulting from the Coriolis effects), the vorticity acceleration outside the wake, and a reduced velocity defect in the centre of the wake. Note that the vortex lines arch over the wake from one side to the other. The depth of the wake is approximately $x^* w^+/U_0$: here w^+ is the vertical velocity which, by continuity, is of the order of $u^+ H/L_R$, where u^+ is of the order of the velocity defect U_0. Hence the upward slope of the wake boundary is of the order of H/L_R which typically is of the order of 10^{-2}, which is very small.

The third term in (41), the lift term, is effective over a distance of order D outside the body if over the whole resistive region there is a net transverse force *on the flow* (see section 2(d)). Because there is then a net circulation Γ set up, i.e. $\iint \Delta\omega \, dx \, dy = \Gamma = \iint G \, dx \, dy$, the integral being defined in any horizontal plane below the top of the mountain. This could be caused by an asymmetrical cross-sectional shape e.g. like that of an aerofoil. We recall that the reason why bound vorticity can be created by a transverse force is that when the flow is started vorticity is shed downwind. Thereafter there is no further shedding of vorticity caused by this force. But if $\iint_A G \, dx \, dy$ is only non-zero when the integral is taken over a *partial area* A_p of the order of D^2, then $\Delta\omega_L$ only affects the flow locally. Thus if there are strong transverse forces at the edges of the mountain, they can affect the flow in these regions.

It has been noted (e.g. Smith 1979) that transverse forces can be caused by the inertial forces associated with the fact that the flow around the mountain takes place on a rotating earth (see also Magnaudet and Eames 2000). This leads to a value for G of the order of ϵ, which is not significant for the parameter range considered here but could be for very large mountains where $\mathbb{R}_0 \sim 1$. For the porous mountains there are significant transverse forces caused by the horizontal transverse velocities (v). Their magnitude in relation to the streamwise drag is of the order of v/U_0. As explained above, these transverse components may be enhanced by the Coriolis effect. Because of the vertical spreading of the velocity perturbation in the domain $\mathcal{D}_R$, caused by the Coriolis forces (or rotational waves of very long length-scale) this circulation induces velocities that decrease away from the mountain much more rapidly than $1/r$—in fact the decrease is proportional to $1/r^3$. This contrasts with the persistent effects of shed vorticity caused by resistance in the streamwise directions, i.e. the second term in (41a).

In physical terms the result is that at the outer edges of an elongated mountain where v is positive and negative either side of the centre line (for $y \gtrless 0$) the positive transverse resistance force (or 'lift') on the mountain leads to an inward transverse force, and therefore negative (anticyclonic) and positive (cyclonic) vorticity where $y \gtrless 0$ (Fig. 7). This adds to the drag-induced velocity (v_0), sweeping round the edges of the mountain.

However there is a larger-scale effect on the flow caused by the net rotationally induced turning of the wind (v_1) as it passes over or through the mountain. This induces a net negative transverse force on the flow and therefore a negative circulation $\Gamma < 0$. Thence an asymmetric streamwise perturbation $u_1^{(L)}$ which amplifies the along-wind speed, i.e. $U_0 + u^+$, over the left-hand part of the mountain, and amplifies the transverse wind speed, i.e. v^+, along the front of the mountain. The anticyclonic circulation induced by rotational transverse resistive forces ($G < 0$) also has an effect on the height of the streamlines, σ. Inspection of (14c) shows that, since $(-\partial G/\partial z) < 0$, there is a general uplift of σ on a scale of the order of $\mathbb{L}_R$ (cf. Smith 1979). As (41) shows, this then slightly reduces the circulation (a second-order effect).

5. Comparison with numerical simulations

The only extensive numerical simulations in a clearly defined flow with low $\mathbb{F}$ and finite R_0 are those of OB1, OB2; they studied the flow over an isolated mountain with a rounded shape having a half-length (D) in the flow direction of 40 km, and half-width $\frac{1}{2}\beta D$ in the perpendicular direction of 200 km. The height H is the variable parameter in their simulation, ranging from 1000 to 5000 m. The incident flow was steady. For some simulations their surface was assumed to be smooth, but in others there was a surface roughness. The 'aerodynamic' roughness length, z_0, on the mountain top was effectively 10 cm or 25 m, but in all cases it was reduced to 10 cm on the flat terrain upwind and downwind of the mountain. The flow was calculated without and with turbulent shear stresses. The Froude and Rossby numbers for the cases we consider here are $\mathbb{F} = 0.37$ and 0.22, with $\mathbb{R}_0 = \infty$ and 2.5 ($\epsilon = 0.4$). Note that the grid elements have a scale Δx, Δy of 10 km.

The first point to note is that for this large mountain (which is a model for a 'chain' or 'envelope' of mountains) the Rossby-scale L_R ranges from about 150 km to 450 km as H varies. Therefore L_R is comparable with the transverse half-width of the mountain. In order to make quantitative comparisons with the theory, we have to estimate the effective magnitude and cross-sectional profile of the resistance of the mountain. Some graphs referred to here were published in OB1, OB2, but some additional computations are presented especially for the case where $\mathbb{F} = 0.22$ (see Figs. 2 and 3).

Let us first consider the characteristic effects in the near field or $\mathcal{D}_F$. Figures 2 and 6 of OB1, OB2 respectively and our Fig. 8 show that when $\mathbb{F} \lesssim 0.5$, for both infinite and finite $\mathbb{R}_0$, in the top layer [T] the streamlines are displaced vertically with strong down-flow on the lee side, and that below this in the middle layer [M] the vertical displacements are small. The thickness of [T] on the lee side is about $1.5\mathbb{F}H$. Internal gravity waves propagate nearly vertically upwards showing that the flow in [T] is similar to that over a low hill, with low slope and with low Froude number $\mathbb{F}_{D^T}$ (based on the length D^T of the cut-off hill), i.e. $\mathbb{F}_{D^T} = U_0/(D^T N) \lesssim 1$. There is also some downward propagation, which affects the matching between the flow in [T] and [M], (NPH). Figures 2 and 1 of OB1, OB2, respectively, for the horizontal and surface flow show the large separated back-flow region extending across the width of the mountain and downwind to the end of the computational domain (which may well affect the size of the recirculation zone). These diagrams also show how the flow splits.

When we come to observe the differences in the computed flows with and without rotation, we can see some significant effects. Figure 1 of OB2 and our Fig. 9(a) and (b) show how the streamlines of the approach flow and the wake flow are diverted to the left (in the northern hemisphere) with a net displacement of the centre-line streamline Δy_ψ

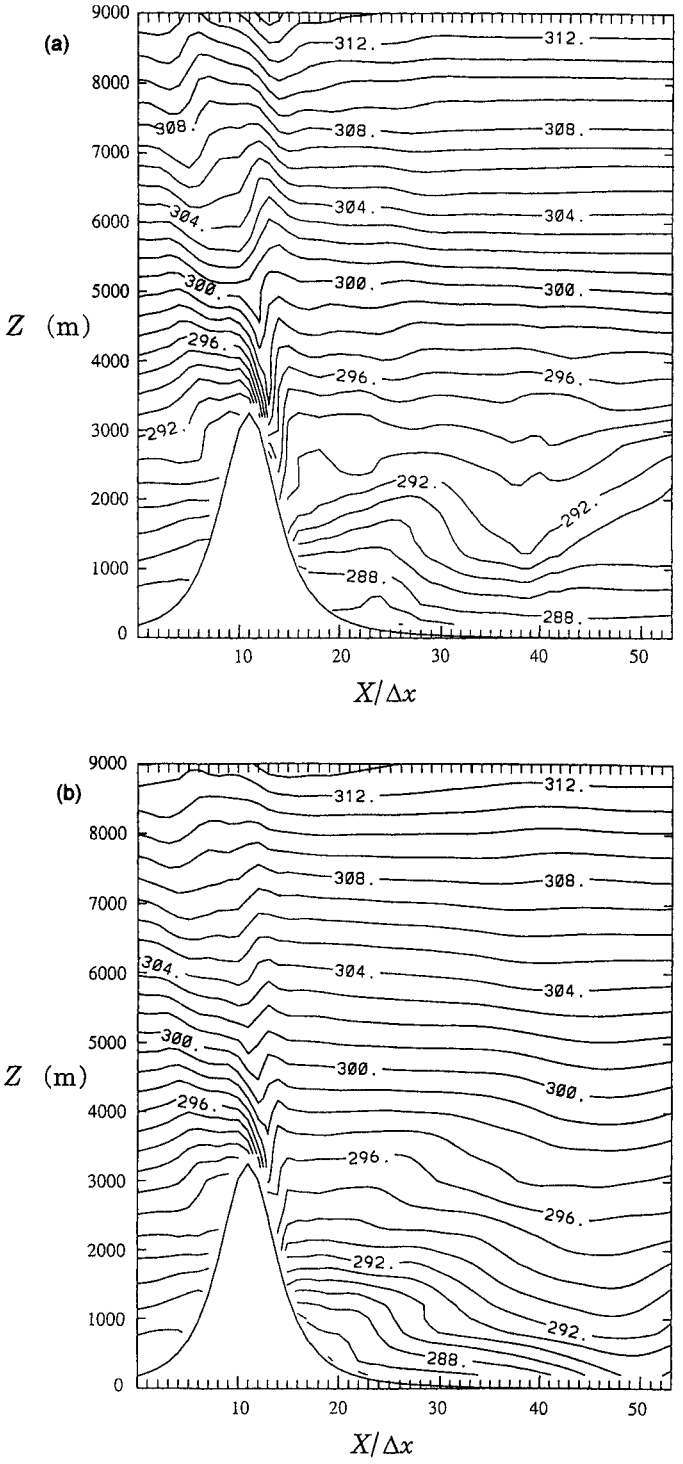

Figure 8. Numerical simulation results for flow over an elliptical mountain, Froude number $\mathbb{F} = 0.22$; Rossby number $\mathbb{R}_0 = 2.5$; showing isentropic surfaces (K) or flow streamlines on x, z planes parallel to the flow. (a) Left side section ($y \simeq 2D$); (b) right side section ($y = -2D$). See text for definitions and discussion.

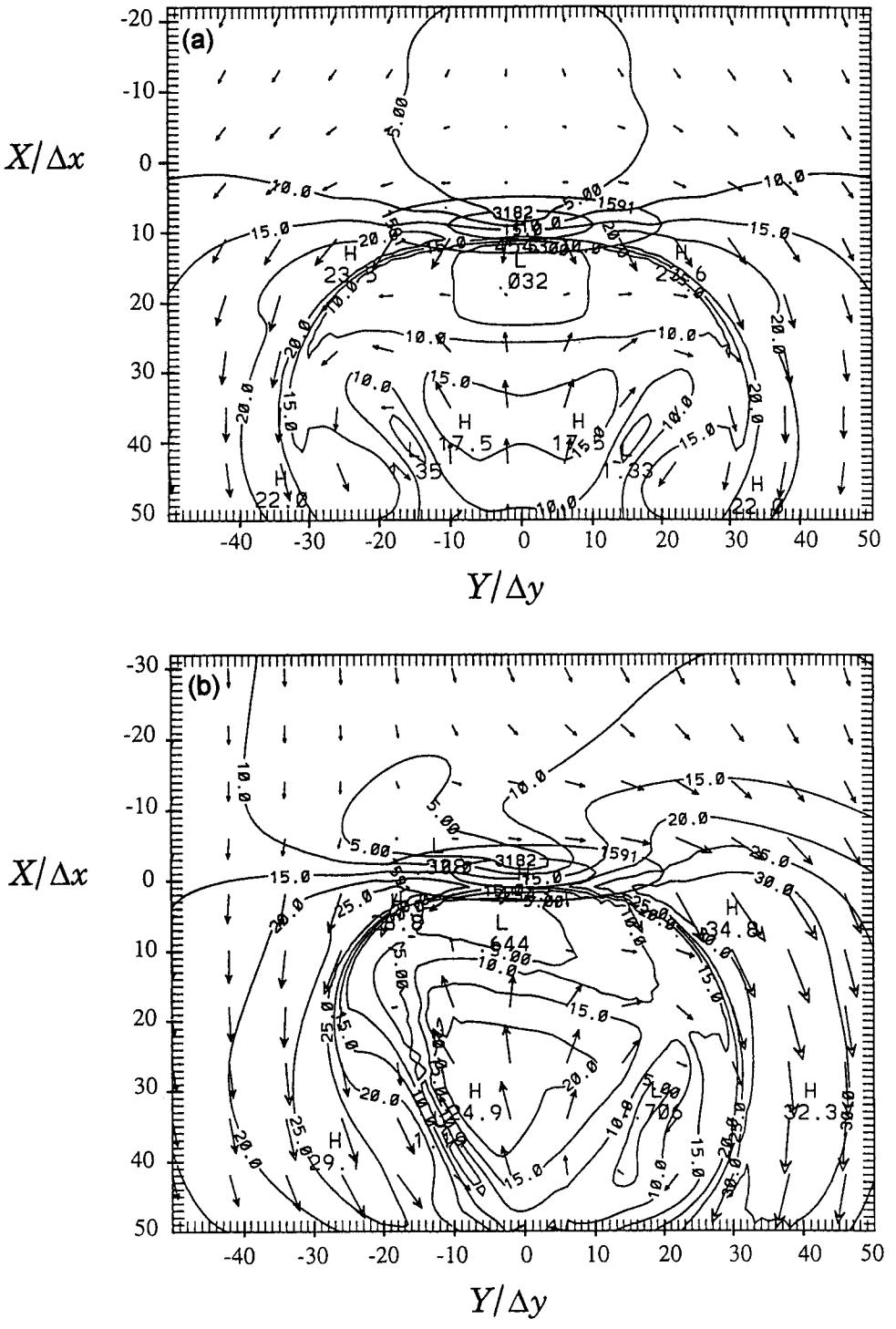

Figure 9. The same case as Fig. 8, showing plan views of velocity vectors and contours of velocity at the surface: (a) Rossby number $\mathbb{R}_0 = \infty$; (b) $\mathbb{R}_0 = 2.5$.

when $\mathbb{R}_0 = 2.5$ and $\mathbb{F} = 0.22$, equal to about $L_R \simeq 450$ km $\simeq \beta D$. This agrees with the theoretical estimate of $\mathbb{F}\Delta y_{\psi(1)}$ in (30) for an elongated mountain taking $\overline{C_D}/2\beta \simeq 3$, as discussed below. The other striking Coriolis effect on the upwind flow is seen in Fig. 1 of OB2, where both the streamwise and transverse velocity components u, v are significantly greater near the windward slopes of the mountain. Upwind of the edges of the mountain they are greater than the approach wind speed U_0. For $\mathbb{F} = 0.4$, it is clear from OB2 that when $\mathbb{R}_0 \simeq 2.5$ the approach flow is not significantly changed until $x^* \simeq -L_R \simeq -\beta D$, whereas for $\mathbb{R}_0 = \infty$ this slow-down occurs further upwind where $x^* = -2\beta D$. Note that the leftward turn of the flow and the strength of the barrier jet is greater when $\mathbb{F} = 0.4$ than when $\mathbb{F} = 0.2$, as shown by (29).

The centre-line value of v on the upwind side is about equal to U_0 the upwind velocity. We note that for our model for an elongated porous mountain where $\mathbb{S} = 2.7$, and $\overline{C_D}/2\beta \simeq 1.0$, $(v_1 + v_1^{(L)}) \simeq 2/3U_0$ (by extension from (40)) for the flow outside the wake.

It is noticeable that in the study of the flow over an axisymmetric body at this value of $\mathbb{R}_0$, no asymmetry is visible (Peng *et al.* 1995, Fig. 3). But for elongated mountains the surface streamline asymmetry is very obvious. The effects of the rotation on the horizontal wind speed and wind vectors are presented in Fig. 1 of OB2 and our Fig. 10(a) and (b) from 400 km upwind to 800 km downwind.

When $\mathbb{F} = 0.4$ the effect of rotation leads to the increase of perturbation wind speed (i.e. u^+) relative to the approach wind, of 1.5 U_0 (i.e. a 150% increase) on the left, outside the recirculating wake (at about 2 half-widths), and of 1.0 U_0 on the right (at about 1.5 half-widths). When $\mathbb{F} = 0.2$, the wind speed increases by about 2.2 U_0 on the left (at about 2 half-widths) and 1.5 U_0 on the right (at about 1.5 half-widths). Note that this increase, which extends for several mountain widths downwind, can be related to the maximum velocity defect. Similar effects have been noted by Doyle and Shapiro (1999).

To simulate the magnitudes of the defect and of the excess perturbation in the wake region, using the porous mountain model it is necessary that the magnitude of the drag coefficient parameter should be increased so that (with reference to (26)) $\overline{C_D}/2\beta \simeq 3$. We note that the average of the velocity increases are, therefore, about 0.5 to 0.6 of the magnitudes of the velocity defect in the wake for $\mathbb{F} = 0.4$, 0.2. In fact, the predicted ratio of the excess to the defect perturbation for the ideal porous mountain is about 0.5, which is quite close!

The speed-up outside the wake is not symmetric, which our model suggests is caused by the lift force acting on the elongated mountain, and is of the right order of magnitude.

The variation of surface pressure without and with rotation are given in Figs. 11 and 12 of OB2 and here in Fig. 10(a) and (b). The large asymmetry of the perturbation pressure (p) is obvious. In OB2 the largest value of the normalized pressure difference in the wake denoted by $\Delta p_w = \{p(x, y \simeq \beta/2, 0) - p(x, y = \beta/2)0\} \simeq 1.3\ \mathbb{S}$, where $\mathbb{S} = 1/\mathbb{F} = 2.7$. In Fig. 11(b), the *largest* difference $\simeq 1.8\ \mathbb{S}$; but taking the average over downwind distances $\Delta p_w \simeq 1.1\ \mathbb{S}$. This difference is taken across a transverse distance of the order of $\beta D (\simeq 400$ km) in the first case and $(1.2\ \beta D)$ 500 km in the second case.

Our analysis shows that in $\mathcal{D}_R$ to leading order in the perturbation there is a geostrophic balance, in which case $\Delta p_w = \Delta p_{w_{gs}}$ where $\Delta p_{w_{gs}} \simeq \epsilon\beta(-\overline{u})$, where $-\overline{u}$ is the *average* defect velocity ($\simeq -1.25$, -1.5 for $\mathbb{F} = 0.4$, 0.2). We find $\Delta p_{w_{gs}} \simeq$ (1.9, 1.7) $\mathbb{S}$ for the two cases. This is consistent with the theoretical model of the porous mountain (in 31; assuming $C_D/2\beta \simeq 3$) which yields $\Delta p_w \simeq 2\ \mathbb{S}$ for these parameters.

There is, of course, a symmetric component to the pressure distribution across the mountains. The pressure drop across the mountain, Δp_M, on the centre line for the

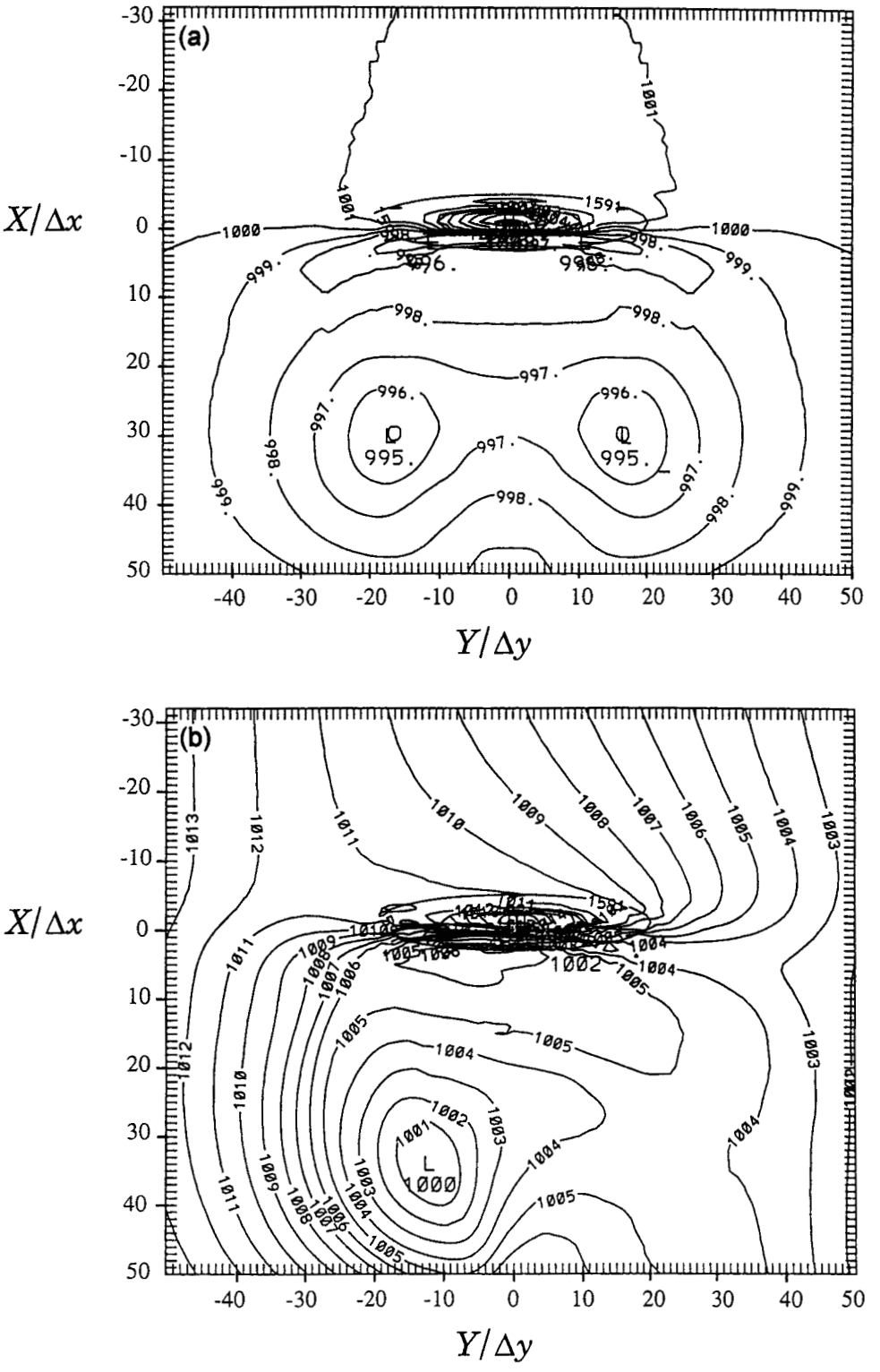

Figure 10. As Fig. 8, but plan views of surface pressure (mb): (a) $\mathbb{R}_0 = \infty$; (b) $\mathbb{R}_0 = 2.5$.

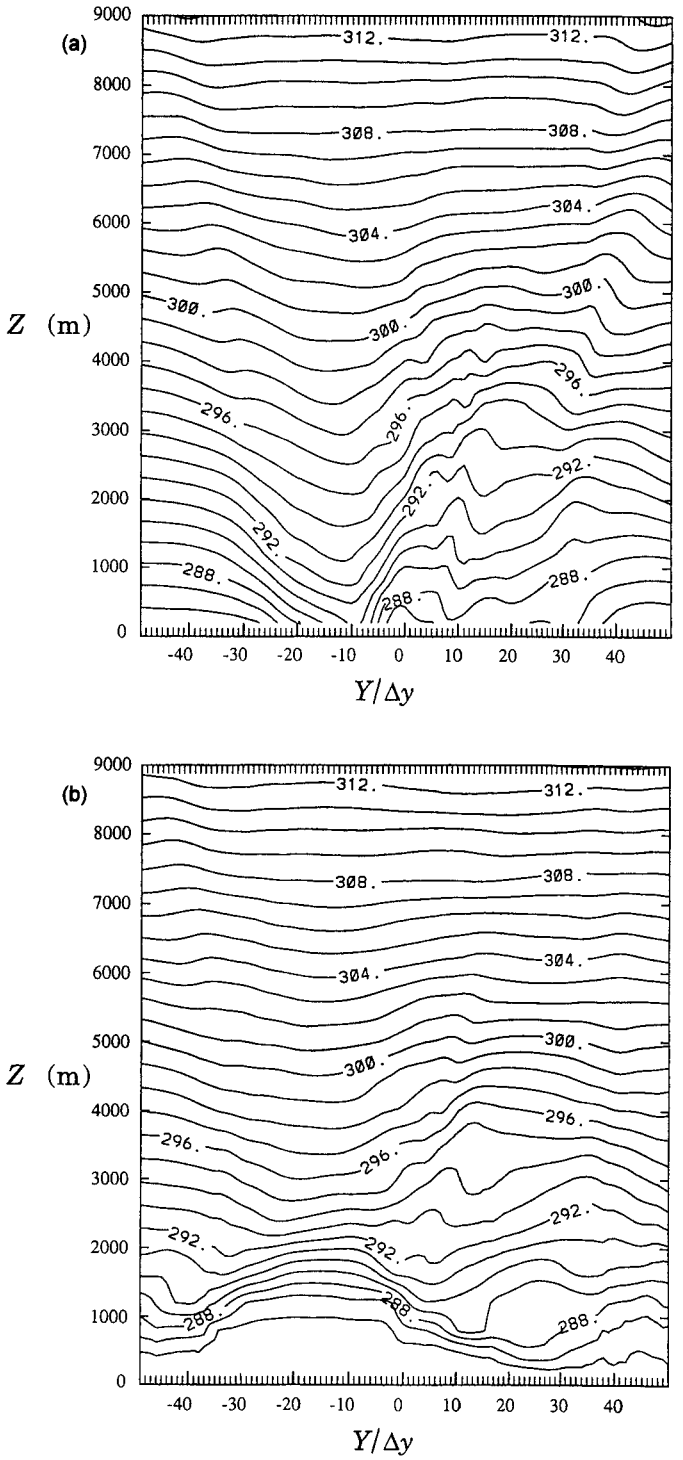

Figure 11. Same case as Fig. 8. Isentropic surfaces (K) in the yz plane 300 km downwind of the mountain, showing the decrease in elevation for $Y < 0$ on the right, and rise for $Y > 0$ on the left, looking downwind: (a) with no surface friction, (b) with surface friction—showing how the main effects are now near the mountain top.

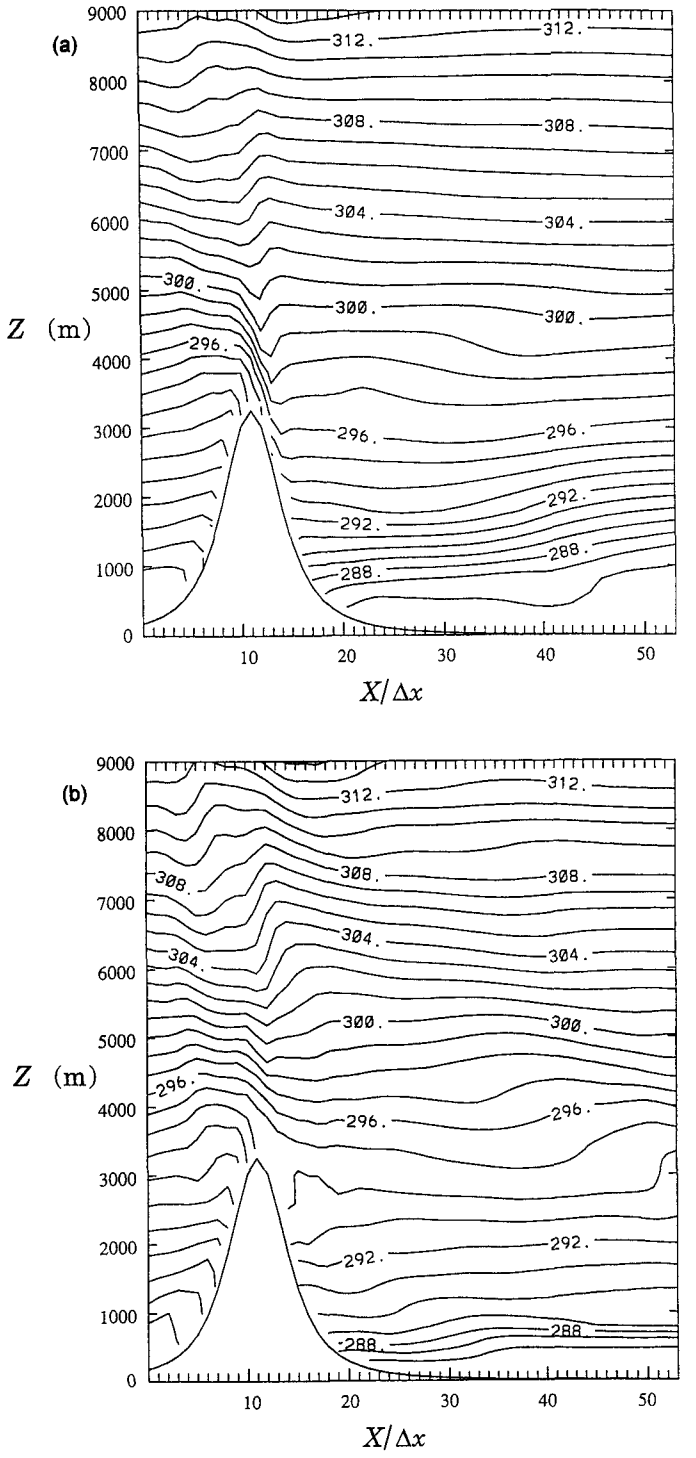

Figure 12. As Fig. 8 but with surface friction. (Roughness length $z_0 = 15$ m at the top of the mountains.)

case of $\mathbb{F} = 0.4$, (Fig. 7 of OB2), is equal to about $3\mathbb{S}$ when $\mathbb{R}_0 = 2.5$, and $2.3\ \mathbb{S}$ when $\mathbb{R}_0 = \infty$.

If this pressure drop is proportional to the strength of the wake perturbations (characterized by the parameter $C_D/\beta \simeq 6$ for best fit) our porous model suggests from (10) that $\Delta p_M \simeq \overline{C_D}/\beta \simeq 6 \simeq 2.4\ \mathbb{S}$ for the case of $\mathbb{F} \simeq 0.4$.

Note that in our conceptual model the pressure drop between the upwind and downwind sides of the mountain, Δp_m, is controlled by local processes so that

$$\Delta p_M \sim \overline{C_D}/\beta \sim 0(1),$$

However the asymmetric pressure across the wake is greater (when $\mathbb{S} \gg 1$), being produced by Coriolis forces over a long range. Its approximate value is

$$\Delta p_w \sim \frac{C_D}{\beta} \cdot \mathbb{S}.$$

But the numerical results in Fig. 10(b) indicate that when $\beta \gg 1$ and $\mathbb{F} \ll 1$, in the near field, the pressure drop and the drag are as large as the far-field values. This is because the rotational forces produce such large lateral pressure changes that they affect Δp_m, possibly through mechanisms associated with the lift correction term $u^{(L)}$.

6. Discussion of main results

The idealized perturbation model presented here approximates many of the main features of the stratified rotating flow over and around mountains when $\mathbb{F} \ll 1$ and $\mathbb{R}_0 \gg 1$. However since the idealized mountain is porous, the model only describes approximately the barrier jet on the upwind side of the mountain analysed by Shutts (1998) and the reverse flow in the wake computed by OB1, OB2. In this concluding section we discuss a few points about related models and limitations of these models. We also consider how it can be applied more widely to mesoscale flows.

The results for the pressure variations on the scale L_R are related to the vertical displacement σ and to the streamwise velocity perturbation because of the hydrostatic and geostrophic balances see Figs. 5(b) and (11). However, they can also be explained in terms of the integral of the Coriolis acceleration, which only converges in the outer region, on the L_R scale. By contrast with the high-Froude-number flow discussed by Smith (1979) and Buzzi and Tibaldi (1977), here at low Froude number the antisymmetric pressure does not decay in the wake downwind. This is because of the persistence downwind of the wake (or PV anomaly), and the geostrophic balance which leads to higher pressure perturbation on the left ($y > 0$). It can also be explained in terms of differential vortex stretching by the upward and downward displacement of streamlines each side of the wake (see section 4). The overall change in the asymmetric pressure, over a distance L_R, is of the order $\rho_{00} U_0^2 \mathbb{F}^{-1}$, which surprisingly is much greater than the dynamic head U_0^2. The magnitude of this pressure drop is independent of the Rossby number (see also Shutts 1998). If there is significant vertical numerical diffusion in a computational model, the wake diffuses on a scale less than L_R, and then these large lateral pressure gradients fail to be simulated. This may be the reason why they have to be parametrized artificially in NWP models (Cullen, personal communication).

The symmetric pressure in the model is of the order of the dynamic head $(1/2\rho_\infty U_0^2)$ and decays downwind, but the actual magnitude of the symmetric pressure drop in the numerical simulation of OB2 is comparable with the antisymmetric pressure change.

Thus the symmetric drag force per unit width, that was assumed by Lott and Miller (1997) to be of the order of $1/\mathbb{F}$, is consistent with the magnitude of the numerical simulations for the symmetric drag force. But it is not consistent with the simulation, nor with our theoretical model, for the large antisymmetric pressure changes. For a wide mountain or mountain chain both these symmetric and antisymmetric pressure changes develop close to the mountain (certainly within the scale of 50 km that is typical of the grids used in NWP models).

As regards lift forces on the mountain and changes of direction of the approach flow, in our model it is assumed that the force on the mountain is related to the local direction of the approach flow. Thus if the outer flow leads to a transverse velocity across the mountain, as it does in our model (of the order of $\mathbb{F}^2/\mathbb{R}_0$), this causes the resistive force to have a transverse component (in the $-y$ direction). This induces a weak anticyclonic motion around the mountain and a symmetric upward displacement over the whole mountain, as also occurs in high-Froude-number flows (Smith 1979). Note that, as is observed for an elongated mountain, a small change in the approach flow direction leads to a large change in the flow around the mountain, and possibly and aerodynamical (rather than rotationally) determined lift force.

What are the consequences of neglecting turbulent shear stresses?

- Models of neutral and stratified turbulent flow over hills (e.g. Hunt and Snyder 1980; Hunt and Richards 1984; Wood 1995) have shown how for low levels of surface roughness the location of separation, a distance x_{sep} downwind of the summit, is approximately equal to $x_{\max}$, the location of the maximum in the local pressure perturbation Δp (rather than its gradient). However, for very rough surfaces, or when z_0 is of the order of l (as occurs in the flow over any real chain of mountains, e.g. where $z_0 \sim 10$–30 m), or for very sharp mountain tops (e.g. Castro *et al.* 1983), x_{sep} is less than $x_{\max}$ and separation tends to occur quite close to the top of the mountain.
- The numerical simulation in Fig. 12(a) for a very rough mountain suggests that the lee wave behaviour is disrupted by the very rough mountain top, and that the downwind flow in [T] is mixed with that in [M]. Since the distribution of the drag profile or shed vorticity of the mountain (subsection 2(a)(iv)) determines the form of the far wake, this is why it is also sensitive to the level of mountain roughness and the shear stresses in the flow.
- These shear stresses also affect the internal processes in the breaking waves, and in shear layers where the flow separates and where the top-layer flow meets the middle layer, but probably do not change the depth of the top layer from being about equal to $(\mathbb{F}H)$.
- Shear stresses affecting the lateral spreading are mainly caused by the large-scale horizontal fluctuating motions in the wake (with an effective intensity of, say, 10% of the mean flow). They determine the peak negative velocity and affect the asymmetric pressure distribution in the recirculating wake. This explains the larger value of $\overline{C}_{\mathrm{D}}/\beta$ needed to model the wake. These stresses only change the width significantly (say by about 100%) over a distance of more than 10 wake widths.
- Finally, our model indicates that the streamwise perturbations, u^+, persist downwind and only decay slowly, unlike the perturbation produced in the transverse velocity and unlike all the velocity fluctuation in high-Froude-number flow. In practice this perturbation is controlled by the shear stress at the surface and Coriolis effects through the well established 'spin-down' process. An Ekman layer is formed with depths of the order of $\delta \sim 0.2\, u_*/f \lesssim 200$ m if $u_* \lesssim 1$ m s^{-1}, where u_* is the friction velocity. This sets up a vertical motion, and induces opposing motions within a mixed-layer depth of

say $\Lambda \sim 1500$ m over a distance

$$x_w \sim \frac{\Lambda^*}{\delta} \cdot \frac{1}{f} U \sim 10^3 \text{ km}.$$

Hence the wake effects of a chain of mountains can extend downwind over a significant, synoptic distance.

The essential results presented here may be applied to mesoscale flows; they are applicable to any resistive region that causes a momentum deficit downwind and deflects the flow up to a finite height, H, in the stratified atmosphere (or oceans) on the mesoscale where $\mathbb{F} < 1$ and $\mathbb{R}_0 > 1$. The most significant effects occur when the lateral scales βD of the disturbances are of the order of the Rossby deformation distance, i.e.

$$\beta D \sim L_R \sim \frac{H/N}{f} \simeq \frac{D}{\mathbb{F}} \times \mathbb{R}_0.$$

These mesoscale 'disturbances' might be a mountain, a mountain range, or mountain and valley system (e.g. the Rhone Valley between the Massif Central and the French Alps where $H > 1.5$ km, or the Cheshire 'gap' in England where $H \sim 200$ m), or a large area where the roughness changes over a finite area (e.g. a peninsula surrounded by sea, such as Kent and the English Channel in a north-easterly stable wind) or a mesoscale convective cloud system moving relative to the crosswind.

In all these cases one finds not only the velocity defect (as is expected when there is no rotation) but a comparable speed-up outside the wake or velocity defect region that cannot be explained by any other mechanism. (The weather forecaster's or climatologist's explanation (e.g. Manley 1952, p. 185) of wind 'channelling', drawn from the analogy of city streets, is not applicable when the channel is 10- to 100-times wider than the mountain either side!) Further detailed study is necessary, but our explanation, based on the 'recovery' outside the defect region of the geostrophic pressure change, is consistent with the observations of the northerly Mistral in the Rhone Valley and the speed-up of the north-east wind in the English Channel, which both occur when the elevated flow is stable.

The other major point of our analysis is that, as a result of rotation, as the air flow approaches the disturbance the air flow rises on the left (or the right facing towards the disturbance) in the northern hemisphere, and descends on the right. This contributes to systematically wetter weather on the left-hand side of mountains/roughness change in the northern hemisphere (if there is a moist prevailing wind), and dryer weather on the right (e.g. compare the wetter north sides of Cumbria and other peninsulas to the dryer south sides). The wetter weather on the right/southern flank of New Zealand's southern Alps is consistent with this concept. (Most climatological books which focus on the upwind and downwind effects, do not mention the lateral variations and never mention Coriolis effects! e.g. Manley 1952, pp. 124–125.)

This concept can also be applied to well developed convective systems in a stable environment, which have a similar effect on the ambient flow as mountains. They tend to move more slowly than the wind because their updraughts contain low-momentum fluid from near the boundary layer. Therefore, like chimney plumes and jets in cross-flows (e.g. Coelho and Hunt 1989) as informal observations from research aircraft have confirmed, these systems tend to block the flow on their upwind side and shed vorticity in their wakes downwind. Where these systems are comparable to the Rossby deformation scale (50 km), because of Coriolis accelerations, they induce rising/descending air on the left/right. Therefore, in a moist atmosphere further convection is likely on the left and less convection on the right.

In the detailed study by Browning and Ludlam (1962) of the 'Wokingham' storm this point was made quite forcibly (their 'right' is our 'left' because they looked towards the storm). Although they commented that the effect might be attributed to Coriolis acceleration, they gave no explanation, nor did they suggest that this is a widespread phenomenon (see also Kropfli and Miller 1976). Of course, the results of this paper are also applicable to other planets where mesoscale phenomena with rotational effects may be even more important.

ACKNOWLEDGEMENTS

Most of this work by JCRH and HO was carried out with support from CERFACS and Météo-France in July to September 1997. JCRH completed the study at ASU with support from NSF, and at the Department of Applied Mathematics and Theoretical Physics, University of Cambridge with support from Trinity College and the Met Office. We are grateful for many useful comments from colleagues, especially Martin Miller, David Stephenson, Paul Mason, Glen Shutts, Jim Rottman and Mike Cullen.

REFERENCES

Aekido, U. and Schär, C.	1998	Low level potential vorticity and cyclogenesis to the lee of the Alps. *J. Atmos. Sci.*, **55,** 186–207
Baines, P. G.	1995	*Topographic effects in stratified flows.* Cambridge University Press, Cambridge, UK
Browning, K. A. and Ludlam, F. H.	1962	Air flow in convective storms. *Q. J. R. Meteorol. Soc.*, **88,** 117–135
Buzzi, A. and Tibaldi, S.	1977	Inertial and frictional effects on rotating and stratified flow over topography. *Q. J. R. Meteorol. Soc.*, **103,** 135–150
Castro, I. P., Snyder, W. H. and Marsh, G. L.	1983	Stratified flow over three-dimensional ridges. *J. Fluid Mech.*, **135,** 261–282
Coelho, S. and Hunt, J. C. R.	1989	Vorticity dynamics of the near field of strong jets in cross flows. *J. Fluid Mech.*, **200,** 95–120
Doyle, J. D. and Shapiro, M. A.	1999	Flow response to large scale topography. *Tellus*, **51A,** 728–748
Drazin, P. G.	1961	On the steady flow of a fluid of variable density past an obstacle. *Tellus*, **8,** 239–251
Gill, A. E.	1982	*Atmosphere–ocean dynamics.* Academic Press, London, UK
Hunt, J. C. R., Feng, Y., Linden, P. F., Greenslade, M. D. and Mobbs, S. D.	1997	Low Froude number stable flows past mountains. *Il Nuovo Cimento*, **20C,** 261–272
Hunt, J. C. R. and Richards, K. J.	1984	Stratified air flow over one or two hills. *Boundary-Layer Meteorol.*, **30,** 223–259
Hunt, J. C. R. and Snyder, W. H.	1980	Experiments on stably and neutrally stratified flow over a model three-dimensional hill. *J. Fluid Mech.*, **96,** 671–704
Hunt, J. C. R., Shutts, G. J. and Derbyshire, S. H.	1996	Stably stratified flows in meteorology. *Dyn. Atmos. Ocean*, **23,** 63–79
Kropfli, R. A. and Miller, L. J.	1976	Kinematic structure and flux quantities in a convective storm from dual Doppler radar observations. *J. Atmos. Sci.*, **33,** 520–529
Lott, F.	1999	Alleviation of stationary biases in a G.C.M. through a mountain drag parameterization scheme and a simple representation of mountain drag. *Mon. Weather Rev.*, **127,** 788–801
Lott, F. and Miller, M. J.	1997	A new subgrid orographic drag parametrization; its formulation and testing. *Q. J. R. Meteorol. Soc.*, **123,** 101–127
Magnaudet, J. and Eames, I.	2000	The motion of high-Reynolds-number bubbles in inhomogeneous flows. *Ann. Rev. Fluid Mech.*, **32,** 659–708
Manley, G.	1952	*Climate and the British scene.* Collins, Glasgow, UK
Mason, P. J.	1977	Forces on spheres moving horizontally in a rotating stratified fluid. *Geophys. Astrophys. Fluid Dyn.*, **8,** 137–154
Meteorological Office	1993	Forecasters Handbook (2nd Edition). The Met. Office, Bracknell UK
Miranda, P. M. A. and James, I. N.	1992	Nonlinear three-dimensional effects on ground wave drag: Splitting flow and breaking waves. *Q. J. R. Meteorol. Soc.*, **118,** 1057–1081

Newley, T. M. J., Pearson, H. J. and Hunt, J. C. R.	1991	Stably stratified rotating flow through a group of obstacles. *Geophys. Astrophys. Fluid Dyn.*, **58,** 147–171
Olafsson, H. and Bougeault, P.	1996	Non-linear flow past an elliptic mountain ridge. *J. Atmos. Sci.*, **53,** 2465–2489
	1997	The effect of rotation and surface friction on orographic drag. *J. Atmos. Sci.*, **54,** 193–210
Peng, M. S., Shang-Wu, L., Chang, S. W. and Williams, R. T.	1995	Flow and mountains: Coriolis force, transient troughs and three dimensionality. *Q. J. R. Meteorol. Soc.*, **121,** 593–613
Scorer, R. S.	1978	*Environmental aerodynamics.* Ellis Horwood, Chichester, UK
Sheppard, P. A.	1956	Airflow over mountains. *Q. J. R. Meteorol. Soc.*, **82,** 528–529
Shutts, G.	1998	Idealised models of the pressure force on mesoscale mountain ridges. *Contrib. Atmos. Phys.*, **71,** 303–313
Smith, R. B.	1979	The influence of earth's rotation on mountain wave drag. *J. Atmos. Sci.*, **36,** 177–180
	1989	Hydrostatic flow over mountains. *Adv. Geophys.*, **31,** 59–81
	1990	Linear theory of stratified flow past an isolated mountain. *Tellus*, **32,** 348–364
Smolarkiewicz, P. K. and Rotunno, R.	1989	Low Froude number flow past three-dimensional obstacles. Part I: Baroclinically generated lee vortices. *J. Atmos. Sci.*, **46,** 1154–1164
Snyder, W. H., Thompson, R. S., Eskridge, R. E., Lawson, R. E., Castro, I. P., Lee, J. T., Hunt, J. C. R. and Ogawa, Y.	1985	The structure of strongly stratified flow over hills: Dividing streamline concepts. *J. Fluid Mech.*, **152,** 249–288
Taylor, G. I.	1994	Air resistance of a flat plate of very porous material. Pp. 383–386 in *Scientific Papers III.* Ed. G. K. Batchelor. Cambridge University Press (1963), UK
Vosper, S. B. and Mobbs, S. D.	1997	Measurement of the pressure field on a mountain. *Q. J. R. Meteorol. Soc.*, **123,** 129–144
Wood, N.	1995	The onset of separation in neutral turbulent flow over hills. *Boundary-Layer Meteorol.*, **76,** 137–64